UNCLASSIFIED

AD NUMBER
AD355573
CLASSIFICATION CHANGES
TO: **UNCLASSIFIED**
FROM: **CONFIDENTIAL**
LIMITATION CHANGES
TO: **Approved for public release; distribution is unlimited.**
FROM: **Distribution authorized to U.S. Gov't. agencies and their contractors; Administrative/Operational Use; DEC 1964. Other requests shall be referred to Air Force Arnold Engineering Development Center, Arnold AFB, TN.**
AUTHORITY
31 dec 1972, per document marking; aedc usaf ltr 14 dec 1973

THIS PAGE IS UNCLASSIFIED

 FDMG

AEDC-TDR-64-236 [redacted]

ARO, INC.
DOCUMENT CONTROL
NO IG-560-343
COPY 79 OF 85
SERIES A PAGES 53

AD-355 573

(TITLE UNCLASSIFIED)

STATIC STABILITY CHARACTERISTICS OF A WINGED BODY WITH VARIOUS INLET CONFIGURATIONS AT MACH NUMBERS OF 2, 5, 8, AND 10

By

R. H. Burt and M. E. Hillsamer
von Kármán Gas Dynamics Facility
ARO, Inc.

TECHNICAL DOCUMENTARY REPORT NO. AEDC-TDR-64-236

December 1964

Program Element 62405334/1366, Task 136608

(Prepared under Contract No. AF 40(600)-1000 by ARO, Inc., contract operator of AEDC, Arnold Air Force Station, Tenn.)

ARNOLD ENGINEERING DEVELOPMENT CENTER

AIR FORCE SYSTEMS COMMAND

UNITED STATES AIR FORCE

[redacted]

04FD-2245

NOTICES

Qualified requesters may obtain copies of this report from DDC, Cameron Station, Alexandria, Va. Orders will be expedited if placed through the librarian or other staff member designated to request and receive documents from DDC.

When Government drawings, specifications or other data are used for any purpose other than in connection with a definitely related Government procurement operation, the United States Government thereby incurs no responsibility nor any obligation whatsoever; and the fact that the Government may have formulated, furnished, or in any way supplied the said drawings, specifications, or other data, is not to be regarded by implication or otherwise as in any manner licensing the holder or any other person or corporation, or conveying any rights or permission to manufacture, use, or sell any patented invention that may in any way be related thereto.

Approved for public release; distribution unlimited.

STATIC STABILITY CHARACTERISTICS OF A WINGED BODY WITH VARIOUS INLET CONFIGURATIONS AT MACH NUMBERS OF 2, 5, 8, AND 10

By

R. H. Burt and M. E. Hillsamer

von Kármán Gas Dynamics Facility

ARO, Inc.

a subsidiary of Sverdrup and Parcel, Inc.

December 1964

ARO Project No. VT0425

References to named commercial products in this report are not to be considered in any sense as an endorsement of the product by the United States Air Force or the Government.

(This abstract is UNCLASSIFIED.)

ABSTRACT

An experimental investigation has been conducted at Mach numbers of 2, 5, 8, and 10 to determine the static stability characteristics of a winged body configuration with various sizes and shapes of inlets attached. Selected results of the longitudinal stability and drag characteristics are presented for each configuration at the various Mach numbers. The effect of inlet position along the model on the aerodynamic characteristics of two inlet configurations is presented for Mach numbers of 8 and 10. The investigation was performed at free-stream unit Reynolds numbers from 0.05 to 0.54 million per inch, angles of attack from -30 to 45 deg, and angles of yaw from 0 to 12 deg.

PUBLICATION REVIEW

This report has been reviewed and publication is approved.

Darreld K Calkins

Darreld K. Calkins
Major, USAF
AF Representative, VKF
DCS/Test

Jean A. Jack

Jean A. Jack
Colonel, USAF
DCS/Test

CONTENTS

TABLES

ILLUSTRATIONS

NOMENCLATURE

A_b	Base area, 13.80 in.^{2}
C_A	Corrected axial-force coefficient, $(C_{A_t} - C_{A_b})$
C_{A_b}	Base axial-force coefficient, $-C_{p_b}(A_b/S)$
C_{A_t}	Total axial-force coefficient, total axial force$/q_\infty S$
C_m	Pitching-moment coefficient referenced to 0.5ℓ, pitching moment$/q_\infty S \bar{c}$
C_{m_α}	Slope of pitching-moment curve $(dC_m/d\alpha)_{\alpha=0}$, 1/deg
C_N	Normal-force coefficient, normal force$/q_\infty S$
C_{N_α}	Slope of normal-force curve $(dC_N/d\alpha)_{\alpha=0}$, 1/deg
C_{p_b}	Base-pressure coefficient, $(p_b - p_\infty)/q_\infty$
$\bar{c}$	Mean aerodynamic chord, 13.80 in. (See Fig. 2)
D	Aerodynamic drag
L	Aerodynamic lift
L/D	Lift-to-drag ratio
$(L/D)_{max}$	Maximum value of L/D
ℓ	Model length, 20 in. (See Fig. 2)
M_∞	Free-stream Mach number
p_b	Base pressure, psia
p_∞	Free-stream pressure, psia
q_∞	Free-stream dynamic pressure, psia
Re_∞	Free-stream unit Reynolds number, 1/in.
S	Wing planform area, 114.8 in.^{2}
x	Distance along model measured from model nose, in.
α	Angle of attack, deg
ψ	Angle of yaw, deg

1.0 INTRODUCTION

At the request of Air Force Flight Dynamics Laboratory (AFFDL), Air Force Systems Command (AFSC), six-component force tests were conducted on a winged body configuration with various sizes and shapes of inlets attached. The tests were performed in the 40-in. supersonic tunnel (Gas Dynamic Wind Tunnel, Supersonic (A)) and the 50-in. Mach 8 and 10 tunnels (Gas Dynamic Wind Tunnels, Hypersonic (B) and (C)) of the von Kármán Gas Dynamics Facility (VKF), Arnold Engineering Development Center (AEDC), AFSC, during the period between November 25, 1963 and August 14, 1964.

The tests objectives were to determine the static stability characteristics of a winged body configuration (previously tested and designated Lockheed WB-3) which was modified to accommodate inlets of various sizes and shapes. The tests were conducted at Mach numbers of 2, 5, 8, and 10 over Reynolds number ranges from 0.081×10^6 to 0.26×10^6 per inch, 0.057×10^6 to 0.543×10^6 per inch, 0.138×10^6 to 0.282×10^6 per inch, and 0.05×10^6 to 0.183×10^6 per inch, respectively. A total of 18 configurations were investigated; however, only seven of these were tested at all four Mach numbers. The tests were conducted over an angle-of-attack range from -30 to 45 deg and yaw angles from 0 to 12 deg.

2.0 APPARATUS

2.1 WIND TUNNELS

2.1.1 Tunnel A

Tunnel A is a 40- x 40-in. continuous flow, closed circuit, variable-density wind tunnel with a Mach number range from 1.5 to 6.0. The top and bottom walls of the nozzle are flexible plates which are automatically positioned at the desired contours by electrically driven screw jacks.

2.1.2 Tunnel B

Tunnel B is a Mach 8, axisymmetric, continuous flow, variable-density wind tunnel with a 50-in.-diam test section. Because of changes in boundary-layer thickness caused by changing pressure level, the

---

Manuscript received October 1964.

contoured nozzle produces an average test section Mach number which varies from 8.0 to 8.1 at stagnation pressures of 100 and 800 psia, respectively,

2.1.3 Tunnel C

Tunnel C is a Mach 10, axisymmetric, continuous flow, variable-density wind tunnel with a 50-in.-diam test section. Because of changes in the boundary-layer thickness caused by changing pressure level, the contoured nozzle produces an average test section Mach number which varies from 10.0 to 10.2 at stagnation pressures of 200 and 2000 psia, respectively.

A unique feature of the tunnel is the model installation chamber below the test section which allows the entire pitch mechanism, sting, and model to be lowered out of the tunnel. When the model is in the retracted position, the fairing doors and the safety doors can be closed, and the tank can be entered for model changes while the tunnel is running. When the model is in the test section, only the fairing doors are closed, and the tank remains at tunnel static pressure.

2.1.4 Air Supply System

The tunnels are powered by the VKF 92,500-hp main compressor system which provides maximum tunnel stagnation pressures of 36 psia at Mach 2, 150 psia at Mach 5, 900 psia at Mach 8, and 2000 psia at Mach 10. To prevent liquefaction of the air in the test sections, the air is heated using heat of compression for the Mach 2 and 5 testing in Tunnel A. A propane-fired heater capable of heating the air to 1360°R is used for Tunnel B, and the propane-fired heater and a 12,000-kw electric heater are used in combination to heat the air to 1900°R for Tunnel C. Details of the tunnels are shown in Fig. 1 and a complete description is given in Ref. 1.

2.2 MODELS AND SUPPORT

The basic model, a winged body configuration, consisted of a 75-deg swept delta wing with a 0.25-in. radius spherical nose and leading edge, a 2.67-deg dihedral on the upper and lower surfaces, and a 6-deg conical half-body on the upper surface. This configuration which was previously tested in Tunnels A and B under the designation Lockheed WB-3 (Ref. 2) was modified to receive various sizes and shapes of inlets. The inlets were basically of eight different geometrical shapes, two of which (numbers 6 and 7) were used to form a single configuration. For each geometrical shape there were two inlets; one with the entrance to the inlet open and another with the entrance closed. An "A" on the inlet number designates the closed inlets. In addition to the different shapes, inlets number 3, 3A, 4, and 4A could be positioned longitudinally along the model in three different positions. Position one indicates the base of the inlet and the base of the model are coincidental, position two, the base of the inlet is 2.5 in. upstream of the base of the model; and position three, the base of the inlet is 5.0 in. upstream of the base of the model. All inlets except numbers 3 and 4 were tested only in position 1. Photographs and details of each configuration are shown in Fig. 2. As shown in the figure inlets number 8 and 8A were attached to the upper surface of the model and the other inlets were attached to the lower surface.

The model was supported in the tunnels by various combinations of bent stings which permitted testing over the angle-of-attack range indicated.

2.3 INSTRUMENTATION

In Tunnel A, a 1.50-in.-diam, force type, six-component, internal, strain gage balance was used to measure aerodynamic forces and moments on the model.

In Tunnels B and C, a 1.00-in.-diam, moment-type, six-component, internal, strain gage balance was used to measure the aerodynamic forces and moments on the model. This balance was cooled by a water jacket which extended over the entire length of the balance. The forward end of the sting was also water cooled. Balance temperatures, measured by chromel-alumel thermocouples, were monitored during the test.

Balance cavity and base pressures were measured by utilizing the standard pressure systems in each tunnel as described in Ref. 1.

3.0 PROCEDURE

3.1 TEST CONDITIONS

The tests were conducted at nominal Mach numbers of 2, 5, 8, and 10 at stagnation pressures from 4 to 12.5 psia, 12 to 150 psia, 360 to 800 psia, and 420 to 1800 psia, respectively. The stagnation temperature was sufficient to prevent liquefaction of the air in the test section at each pressure level. A complete tabulation of the test conditions is given in Table 1 and the test run summary in Table 2.

3.2 DATA REDUCTION

The data reduction was performed with an IBM 7074 digital computer. Interactions between the balance forces were determined during the balance calibrations and used in the calculations to correct recorded values. The forces were also corrected for model weight and model attitudes were corrected for sting deflection. Base pressure corrections were made on the axial-force coefficients. The pitching- and yawing-moment coefficients were referenced about model station $x/\ell = 0.5$, and the model planform area and mean aerodynamic chord were used to reduce the forces and moments to coefficient form.

4.0 RESULTS AND DISCUSSION

The basic aerodynamic characteristics of each configuration are presented in Figs. 3 through 10, the effect of inlet location on stability is shown in Fig. 11, and the stability derivatives and $(L/D)_{max}$ for the seven configurations tested at Mach 2, 5, 8, and 10 are presented in Fig. 12.

The data in Figs. 3 through 10 are presented for the maximum Reynolds number obtained on each configuration. The maximum value of Reynolds number was generally determined at the higher angles of attack by balance load limitations rather than tunnel operating conditions. These data are presented for general interest where it might be desirable to determine the effect of any one inlet on the basic configuration (WB-3). The effect of Reynolds number on the aerodynamic characteristics of configurations WB-3, WB-$3I_3P_1$, and WB-$3I_8$ was investigated over the range available and found to be negligible except for substantial increases in C_A on the inlet configurations at Mach 10 at the lower Reynolds number. Although not shown herein, the largest Reynolds number effect on C_A occurred at $\alpha = 0$ and gradually decreased with increasing angle of attack, becoming insignificant above 15 deg angle of attack. A mismatch in C_A occurred near an angle of attack of 15 deg at $M_\infty = 2$ and 5 on configurations WB-3, WB-$3I_3P_1$, WB-$3I_{3A}$, WB-$3I_4P_1$, and WB-$3I_8$ and is attributed to sting interference. At Mach 2 and 5, a 15-deg offset sting was used to extend the angle of attack on these configurations from 15 to 30 deg. Reynolds number effect was ruled out as a cause for the mismatch as the variation occurred on both open and closed inlet configurations when the Reynolds number was constant for both stings ($\alpha = 0$ to 15 deg and $\alpha = 15$ to 30 deg). As shown in Figs. 4 through 10, the closed inlet configurations resulted in slightly more stable configurations at the lower angles of attack with large increases in C_A and corresponding decreases in L/D at all angles of attack.

The effect of inlet location on the stability of configurations utilizing inlets number 3 and 4 are shown in Fig. 11 for Mach 8 and 10. Moving the inlet forward resulted in slightly less stable configurations for both inlets at both Mach numbers; however, the decrease in stability because of moving the inlet forward is larger for inlet number 4 (Fig. 11b) than inlet number 3 (Fig. 11a).

In Fig. 12 the effect of Mach number on C_{N_α} and C_{m_α} is presented. This figure shows a decreasing normal-force derivative with increasing Mach number and shows that the inlet configurations are slightly more stable than the basic configuration at all Mach numbers except Mach 2. At Mach 2 configurations WB-3I_1, WB-3I_3P_1, WB-3I_{3A}, and WB-3I_4P_1 are slightly less stable. The trend of decreased stability with increasing Mach number is essentially the same for each configuration; however on configuration WB-3I_{3A} the stability does not decrease quite as rapidly with Mach number because of the closed inlet. These curves also show that the stability characteristics of the rectangular inlets follow similar trends regardless of the width or depth of the inlet. The center of pressure as determined from the C_{N_α} and C_{m_α} values indicated a maximum rearward shift of approximately five percent of the model length from model station $x/\ell = 0.65$ as a result of configuration or Mach number variation. The effect of Mach number on $(L/D)_{max}$ is also presented in Fig. 12. The maximum lift-to-drag ratio decreases with an increase in Mach number as expected. The largest decrease in $(L/D)_{max}$ with Mach number occurred on configuration WB-3 while configuration WB-3I_{3A} was affected the least by Mach number.

The values of $(L/D)_{max}$ would be more meaningful, though somewhat smaller, if the model had been tested with control surfaces so that trimmed values of $(L/D)_{max}$ could have been obtained. Also, the trimmed values of (L/D) obtained for the model without control surfaces are at such a low angle of attack that they lack meaning.

REFERENCES

1. Test Facilities Handbook, (5th Edition). "von Kármán Gas Dynamics Facility, Vol. 4." Arnold Engineering Development Center, July 1963.

2. Rockhold, Vernon G., Onspaugh, Carl M., and Marcy, William L. "Study to Determine Aerodynamic Characteristics on Hypersonic Re-Entry Configurations, Part 1, Experimental Phase." WADD Technical Report 61-56, March 1961, Vols. I and II. (CONFIDENTIAL)

TABLE 1
TEST CONDITIONS

M_∞	p_o, psia	T_o, °R	Re x 10^{-6}/in.
2.00	4.0	563	0.081
1.98	7.0	563	0.144
1.98	12.5	563	0.260
4.99	12.3	550	0.057
	68.0	642	0.248
	150.0	642	0.543
8.06	360	1285	0.138
8.09	800	1340	0.282
10.09	420	1740	0.050
10.18	1800	1900	0.183

TABLE 2

TEST RUN SUMMARY

Configuration	M_∞	$Re_\infty \times 10^{-6}$/in.	α Range, deg	ψ Range, deg
WB-3	2	0.260	-5 to +25	0
			0	
		0.144	+10 to +30	0
		0.081	-5 to +15	0
			0	0 to +12
	5	0.543	-5 to +30	0
			0	0 to +12
		0.057	-5 to +15	0
			0	0 to +12
	8	0.282	-3 to +15	0
		0.138	-3 to +45	0
	10	0.183	-12 to +35	0
			0	0 to +12
		0.050	-12 to +45	0
			0	0 to +12
WB-3I_1	2	0.260	-5 to +15	0
			0	0 to +12
		0.081	-5 to +15	0
			0	0 to +12
	5	0.543	-5 to +15	0
			0	0 to +12
	8	0.282	-3 to +27	0
	10	0.183	-5 to +18	0
			0	0 to +12
WB-3I_2	8	0.282	-3 to +27	0
	10	0.183	-5 to +18	0
WB-3I_3P_1	2	0.260	-5 to +25	0
			0	0 to +12
			-5 to +14	+3, +6
		0.144	+10 to +30	0
		0.081	-5 to +15	0
			0	0 to +12
	5	0.543	-5 to +30	0
			0	0 to +12
			-5 to +14	+3, +6
		0.057	-5 to +15	0
			0	0 to +12
WB-3I_3P_1	8	0.282	-3 to +27	0
			0	0 to +12
		0.138	-3 5o +45	0
	10	0.183	-5 to +34	0
			0	0 to +12
			-5 to +15	+3, +6
		0.050	-5 to +18	0
			0	0 to +12

TABLE 2 (Continued)

Configuration	M_∞	$Re_\infty \times 10^{-6}$/in.	α Range, deg	ψ Range, deg
WB-3I_3P_2	8	0.283	-3 to +27	0
			0	0 to +12
		0.138	+15 to +45	0
	10	0.183	-5 to +34	0
			-5 to +15	+3, +6
WB-3I_3P_3	8	0.283	-3 to +27	0
			0	0 to +12
		0.138	+15 to +45	0
	10	0.183	-5 to +37	0
			0	0 to +12
			-5 to +15	+3, +6
WB-3I_4P_1	2	0.260	-5 to +26	0
			0	0 to +12
		0.144	+10 to +30	0
		0.081	-5 to +15	0
			0	0 to +12
	5	0.543	-5 to +30	0
			0	0 to +12
	8	0.282	-3 to +27	0
			0	0 to +12
		0.138	+15 to +45	0
	10	0.183	-5 to +18	0
			0	0 to +12
WB-3I_4P_3	8	0.282	-3 to +27	0
			0	0 to +12
		0.138	+15 to +45	0
	10	0.183	-5 to +34	0
			0	0 to +12
WB-3I_5	5	0.543	-5 to +15	0
			0	0 to +12
	10	0.183	-5 to +18	0
WB-3$I_{6\ \&\ 7}$	2	0.260	-5 to +15	0
			0	0 to +12
			-5 to +14	+3, +6
	5	0.543	-5 to +15	0
			0	0 to +12
			-5 to +14	+3, +6
	8	0.282	-3 to +27	0
	10	0.183	-5 to +18	0
			0	0 to +12
			-5 to +15	+3, +6

TABLE 2 (Concluded)

Configuration	M_∞	$Re_\infty \times 10^{-6}$/in.	α Range, deg	ψ Range, deg
WB-3I_8	2	0.260	-25 to +15	0
			0	0 to +12
			-5 to +14	+3, +6
		0.144	-30 to -10	0
		0.081	-5 to +15	0
			0	0 to +12
	5	0.543	-30 to +15	0
			0	0 to +12
			-5 to +14	+3, +6
		0.057	-5 to +15	0
			0	0 to +12
	8	0.282	-12 to +30	0
			0	0 to +12
	10	0.183	-30 to +15	0
			0	0 to +12
			-5 to +15	+3, +6
		0.050	-12 to +15	0
			0	0 to +12
WB-3I_{1A}	5	0.543	-5 to +15	0
	10	0.183	-5 to +15	0
WB-3I_{2A}	5	0.543	-5 to +15	0
	10	0.183	-5 to +18	0
WB-3I_{3A}	2	0.260	-5 to +25	0
			0	0 to +12
		0.144	+10 to +30	0
		0.081	-5 to +15	0
			0	0 to +12
	5	0.543	-5 to +15	0
			0	0 to +12
		0.248	+10 to +30	0
		0.057	-5 to +15	0
			0	0 to +12
	8	0.282	-3 to +27	0
		0.138	+15 to +45	0
	10	0.183	-5 to +32	0
WB-3I_{4A}	10	0.183	-5 to +15	0
(This configuration was to be tested at $M_\infty = 5$, but the inlet failed)				
WB-3I_{5A}	5	0.543	-5 to +30	0
	10	0.183	-5 to +18	0
WB-3I_{6A} & 7A	5	0.543	-5 to +15	0
	10	0.183	-5 to +18	0
WB-3I_{8A}	5	0.543	-5 to +30	0
	10	0.183	-12 to +15	0

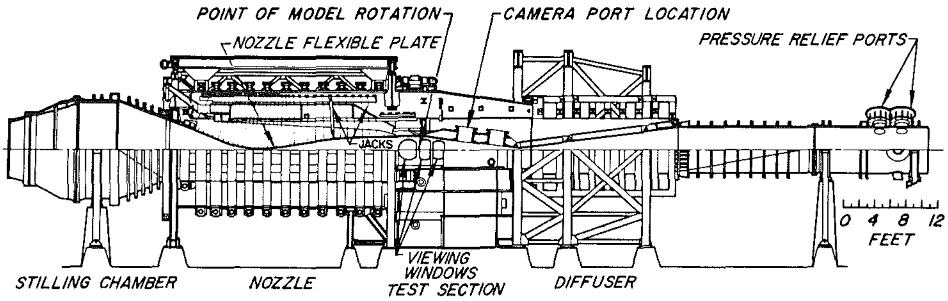

Assembly

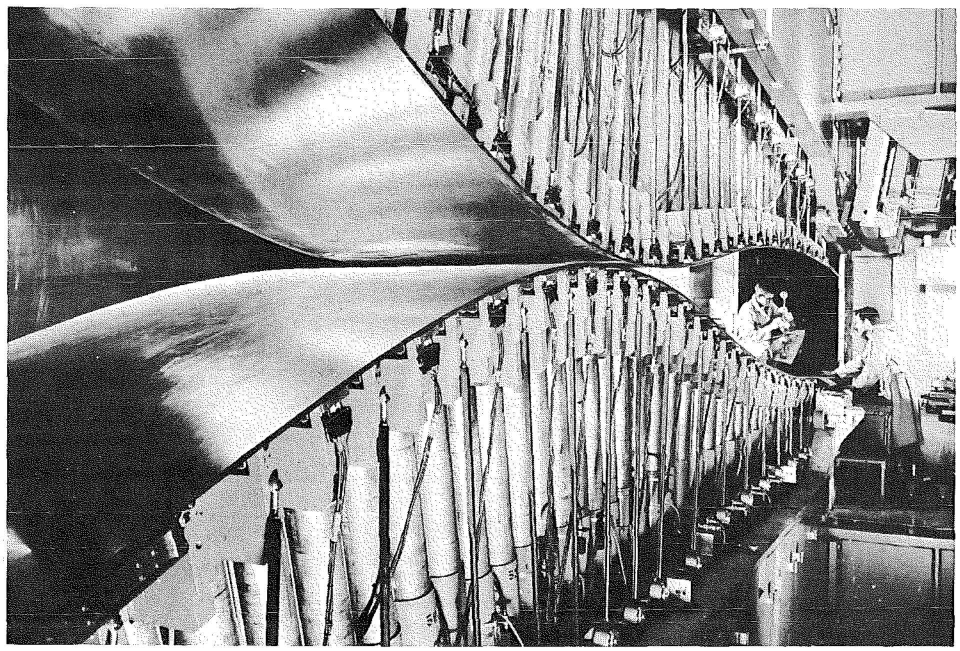

Nozzle and Test Section

a. Tunnel A

Fig. 1 Wind Tunnels

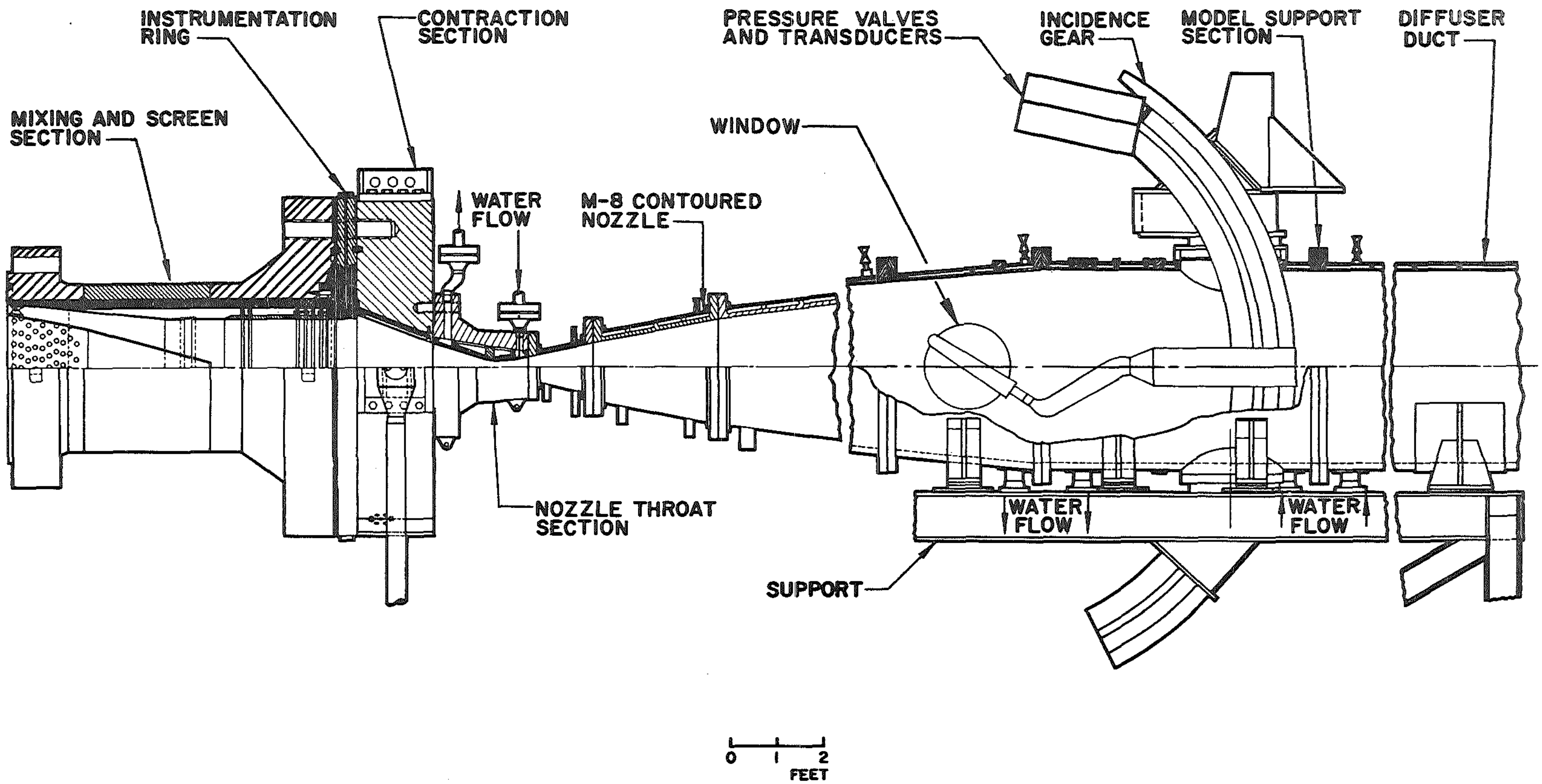

b. Tunnel B

Fig. 1 Continued

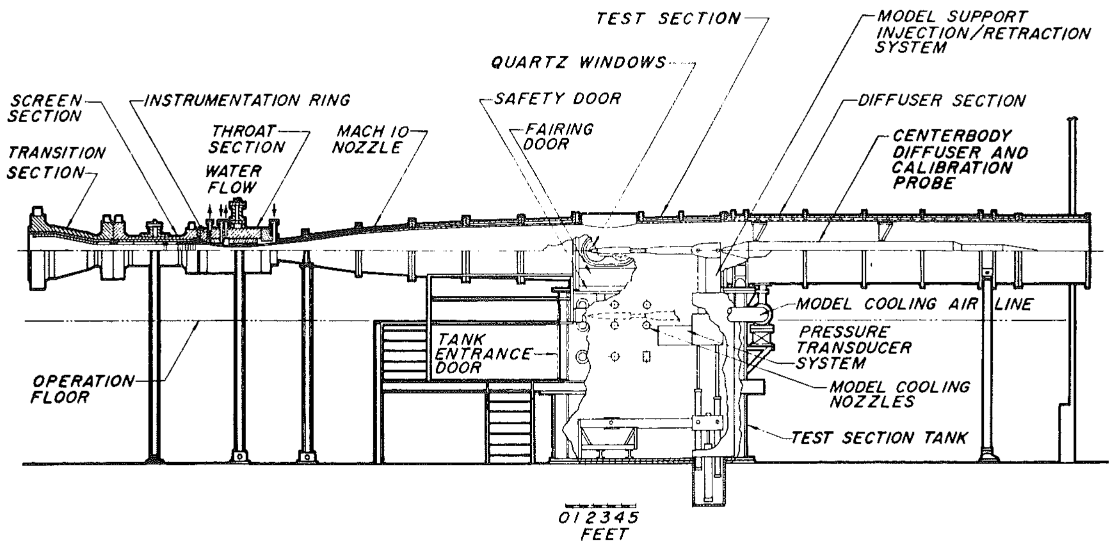

Tunnel Assembly

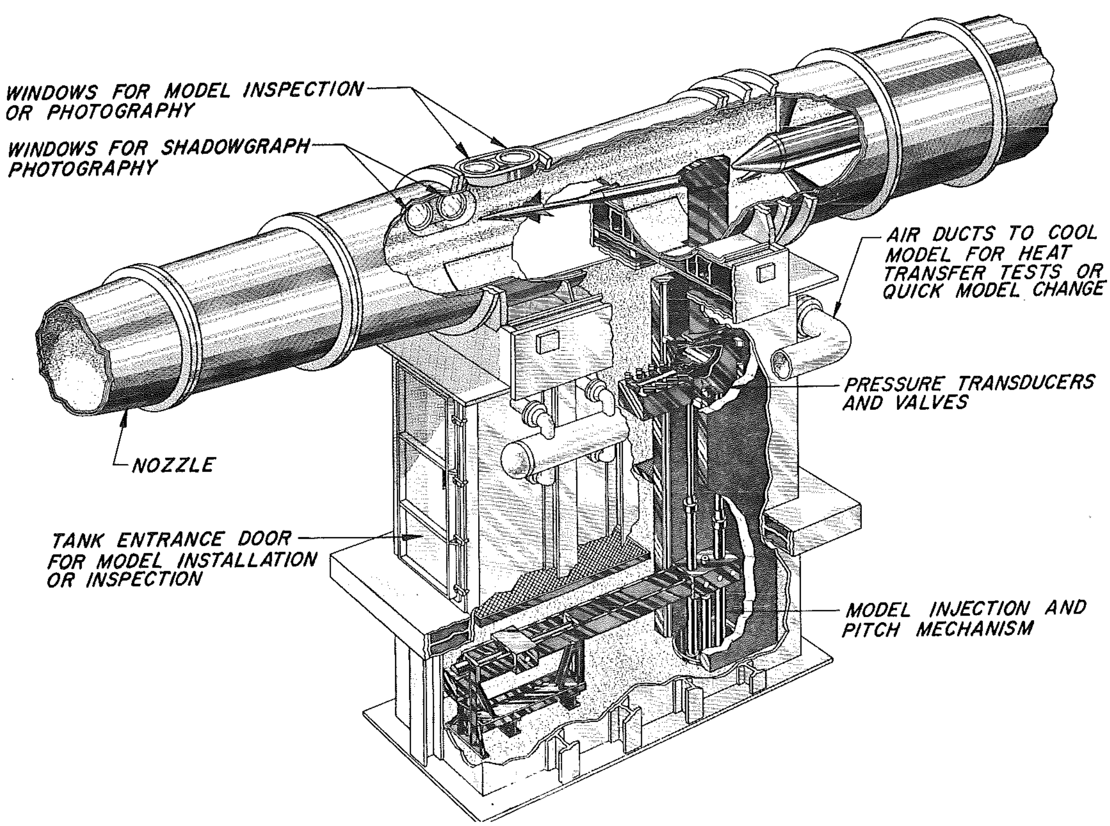

Tunnel Test Section

c. Tunnel C

Fig. 1 Continued

d. Typical Model Installation

Fig. 1 Concluded

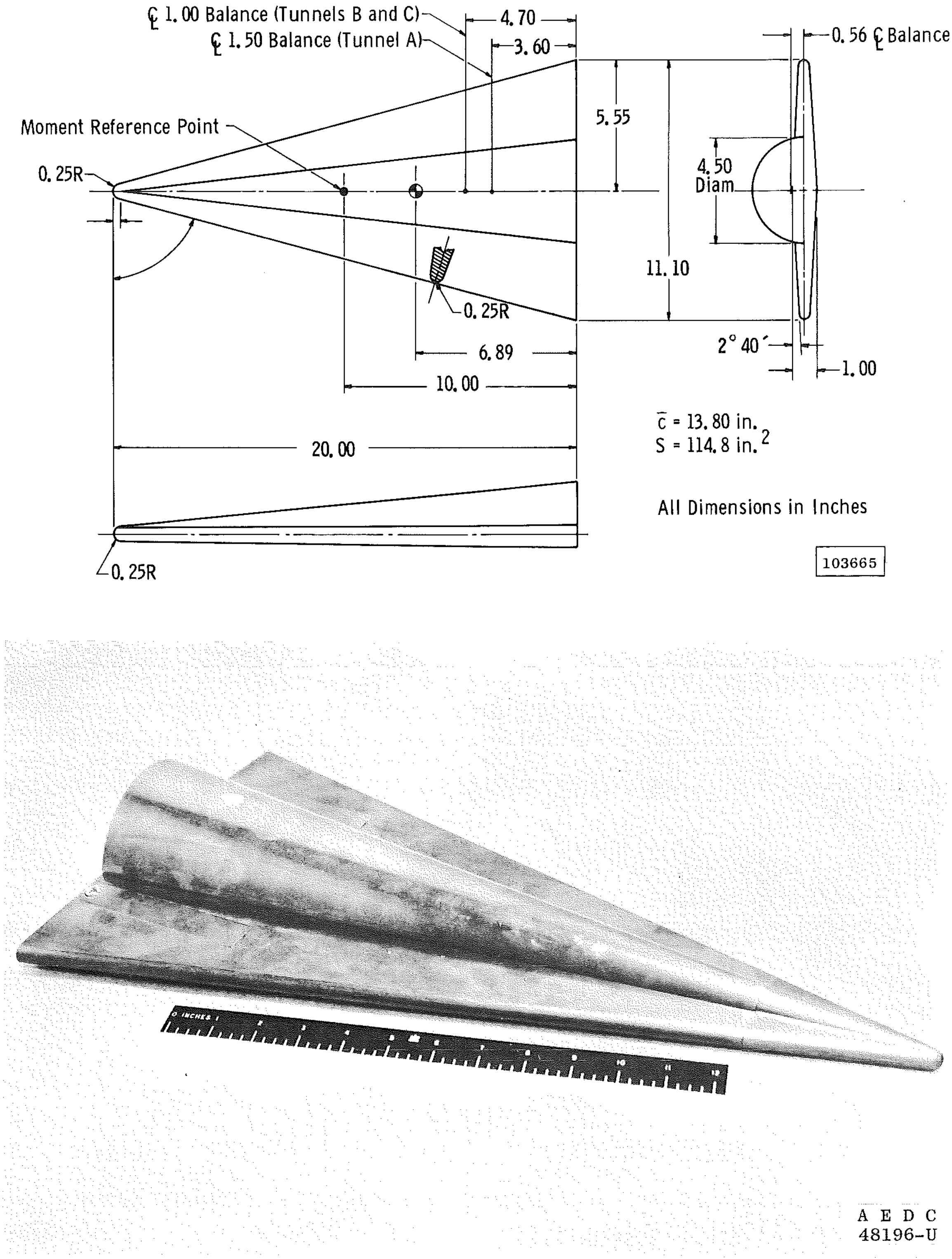

a. Configuration WB-3

Fig. 2 Configuration Details

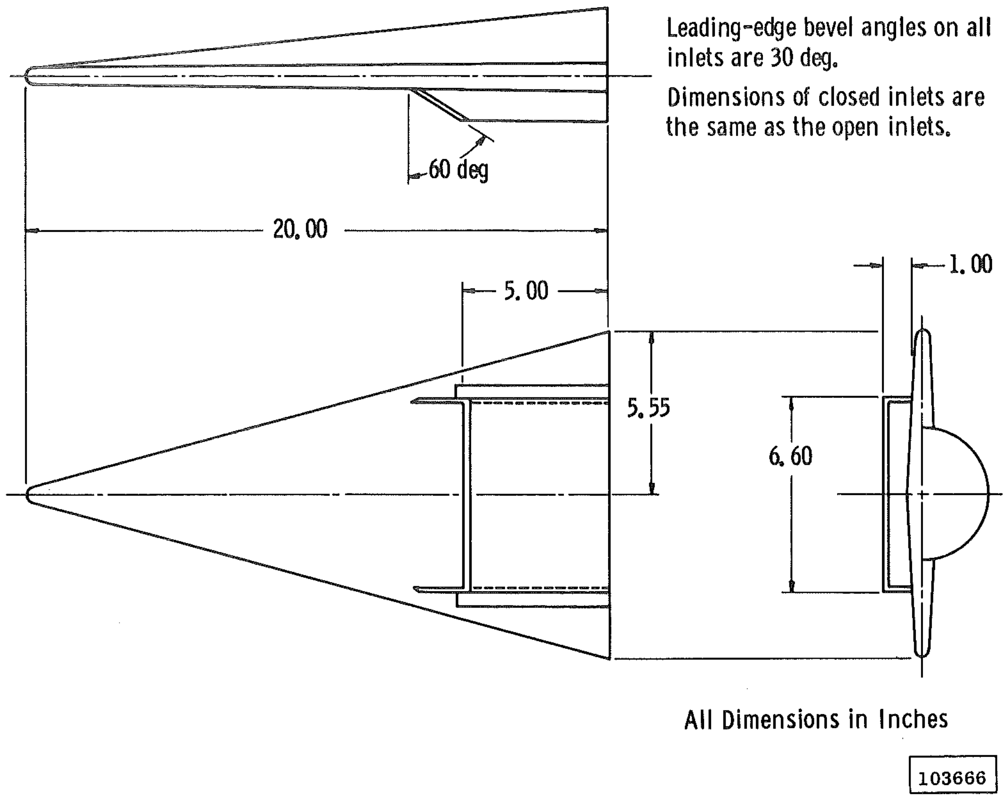

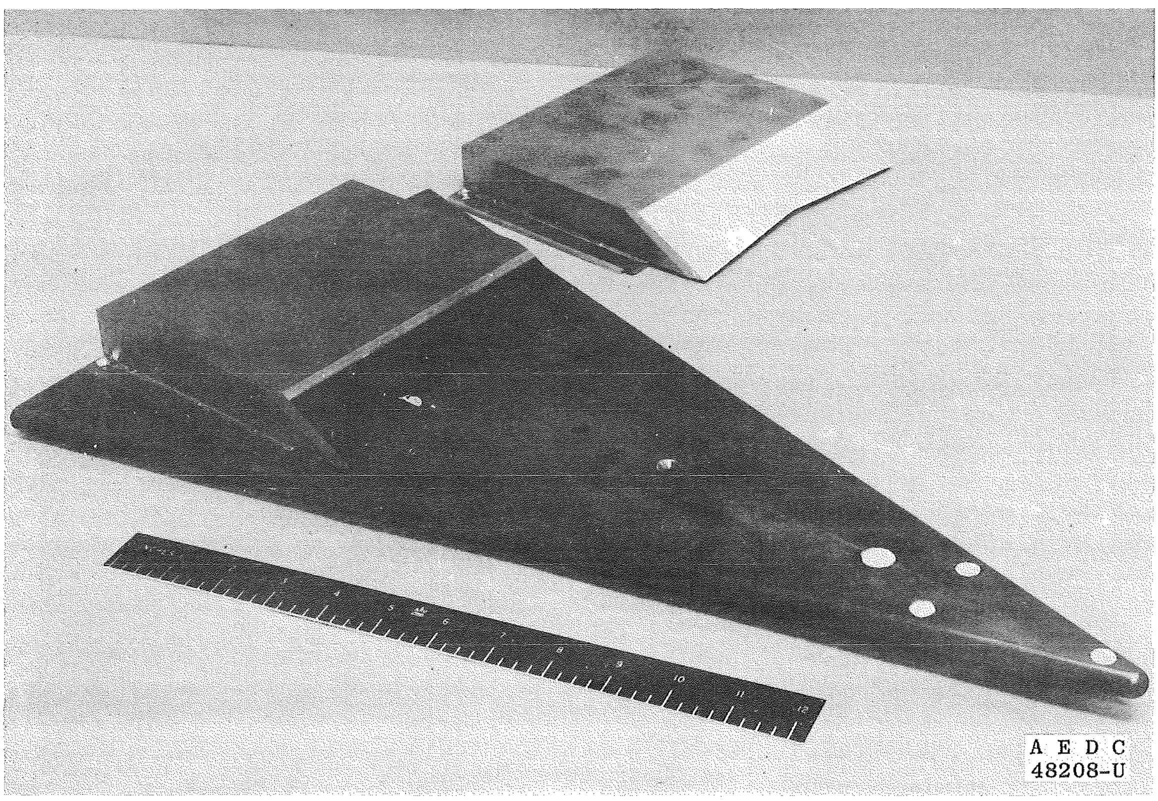

b. Configurations WB-3I$_1$ and WB-3I$_{1A}$

Fig. 2 Continued

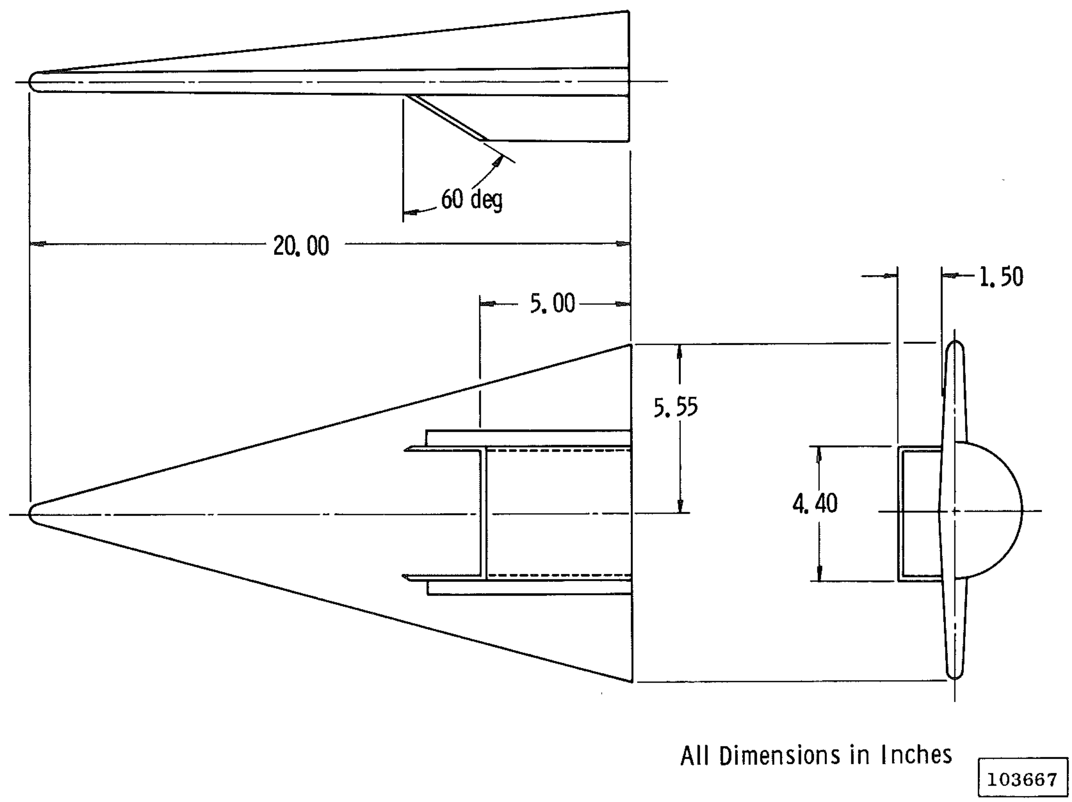

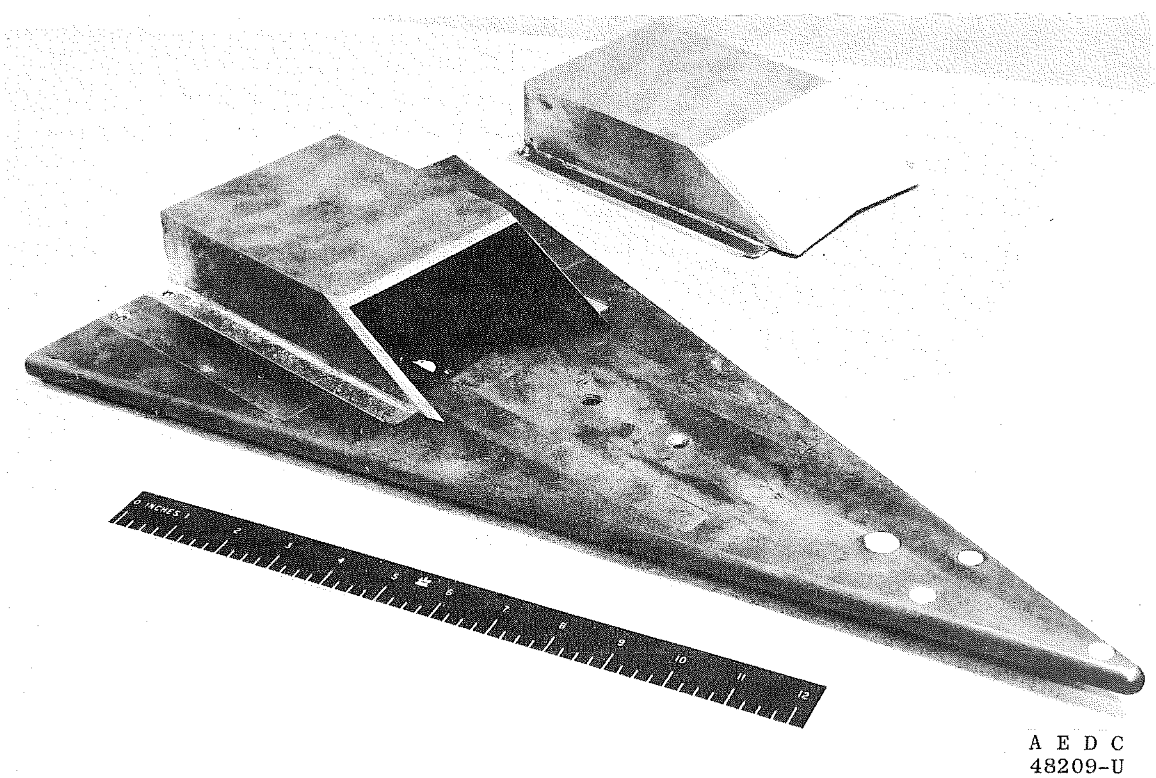

c. Configurations $WB\text{-}3I_2$ and $WB\text{-}3I_{2A}$

Fig. 2 Continued

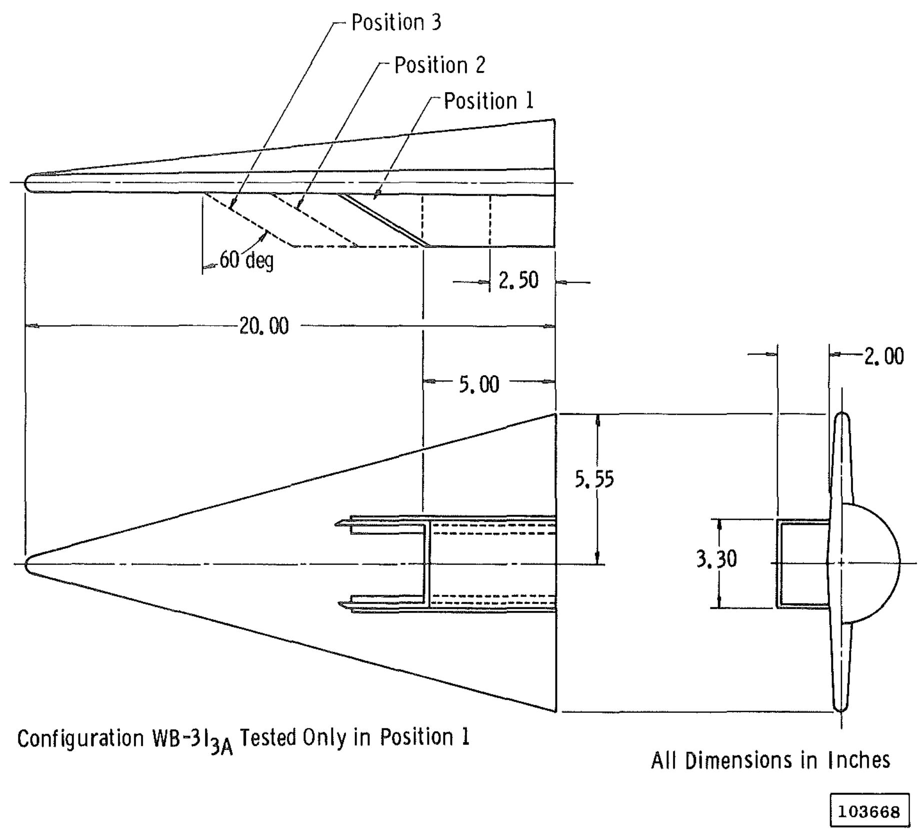

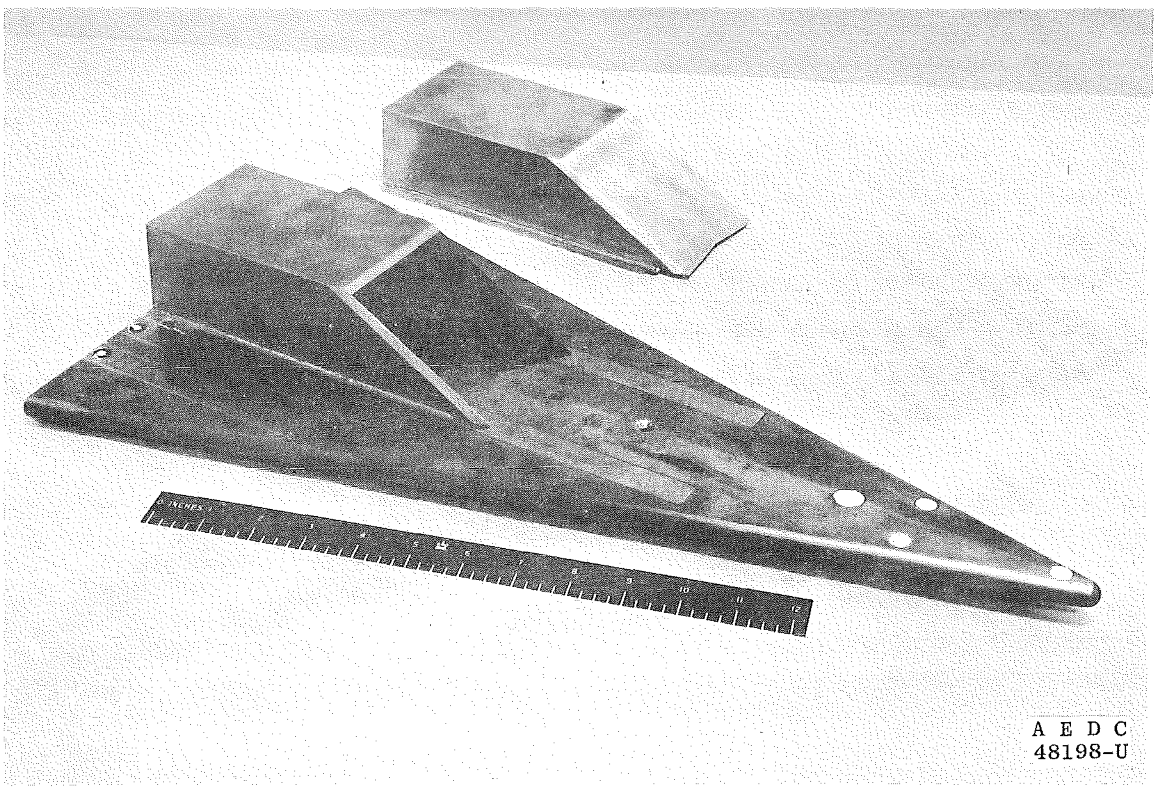

d. Configurations WB-3I3 P1, WB-3I3 P2, WB-3I3 P3, and WB-3I3A

Fig. 2 Continued

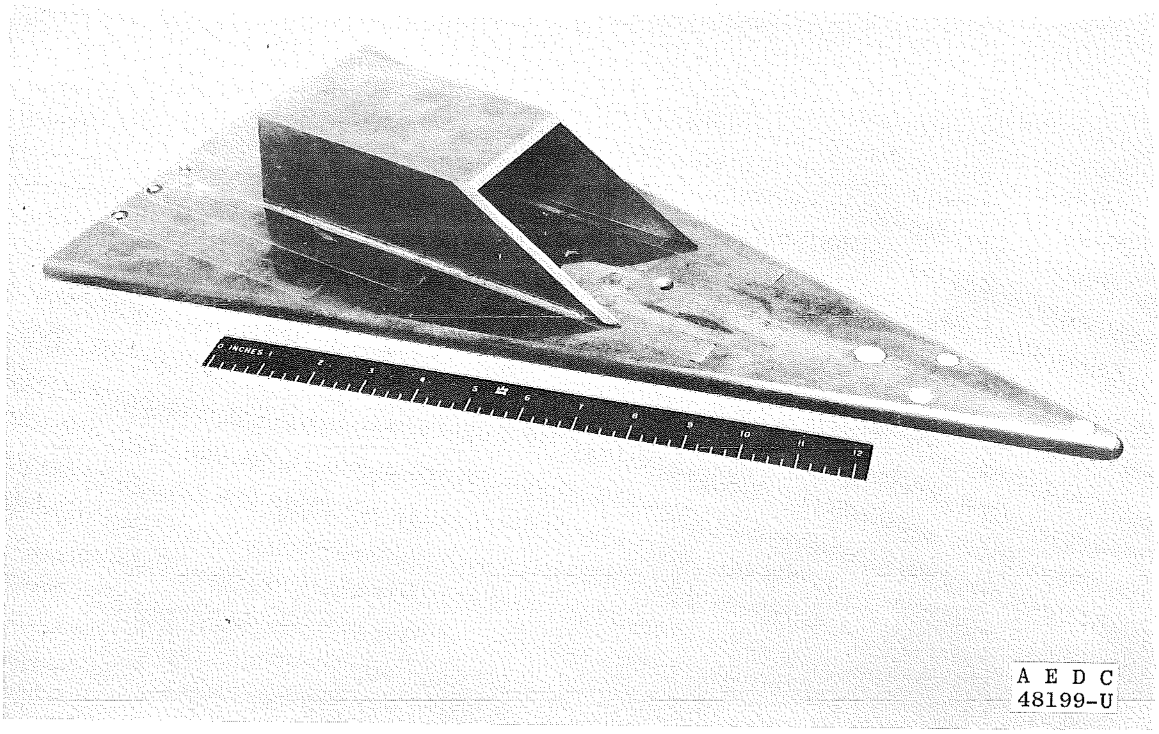

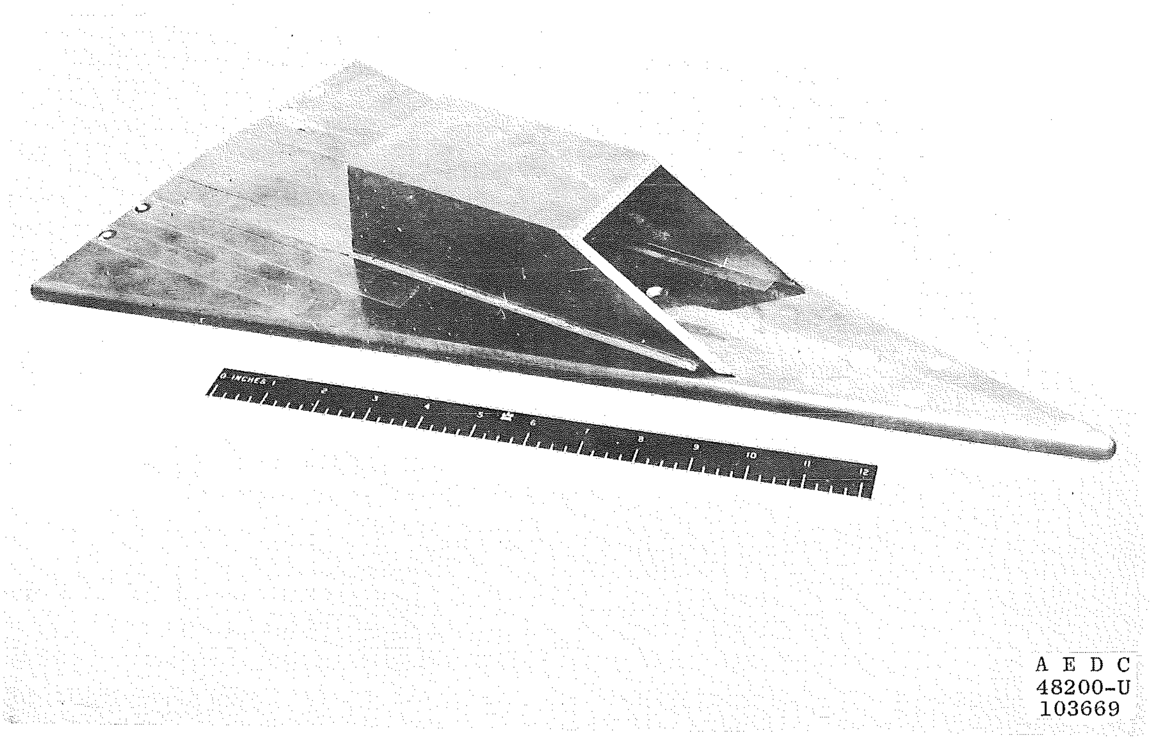

d. Concluded

Fig. 2 Continued

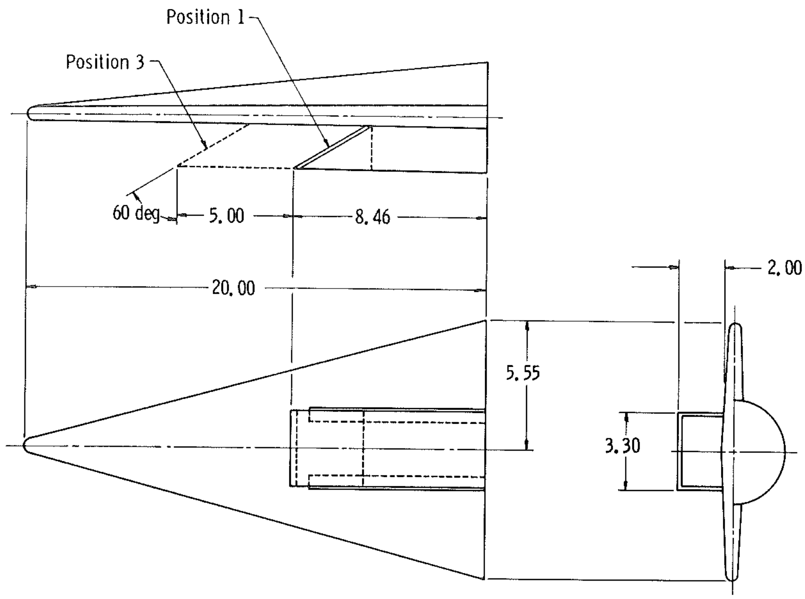

Configuration WB-3I$_{4A}$ Tested Only in Position 1

All Dimensions in Inches

103670

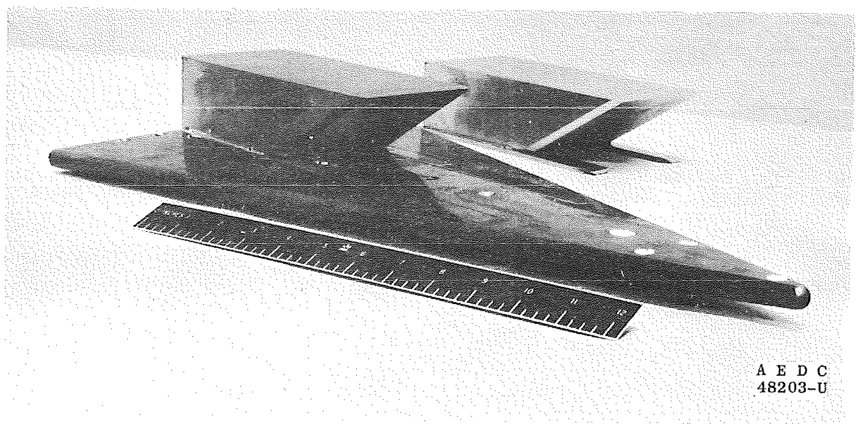

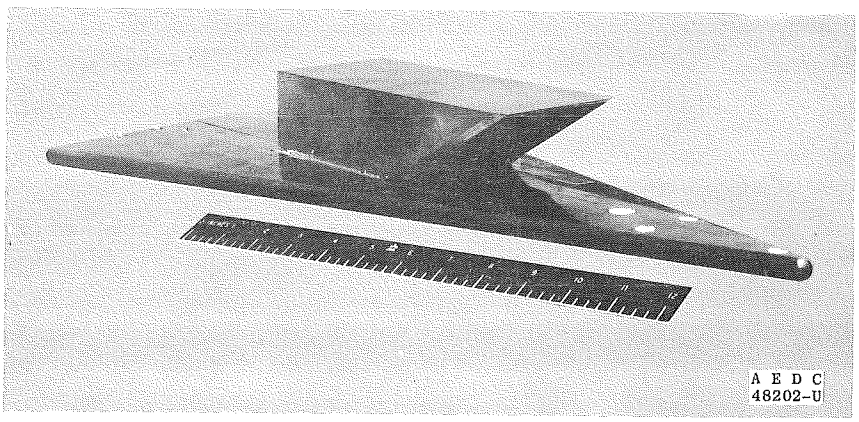

e. Configurations WB-3I$_4$ P$_1$, WB-3I$_4$ P$_3$, and WB-3I$_{4A}$

Fig. 2 Continued

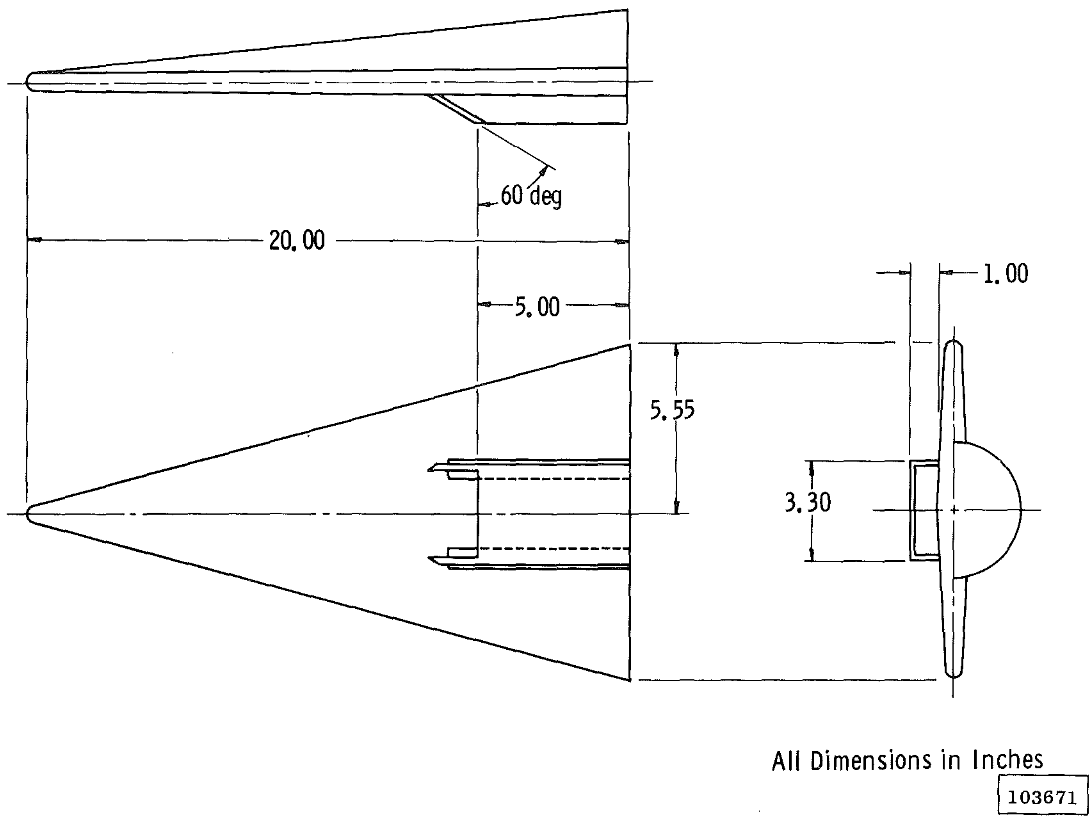

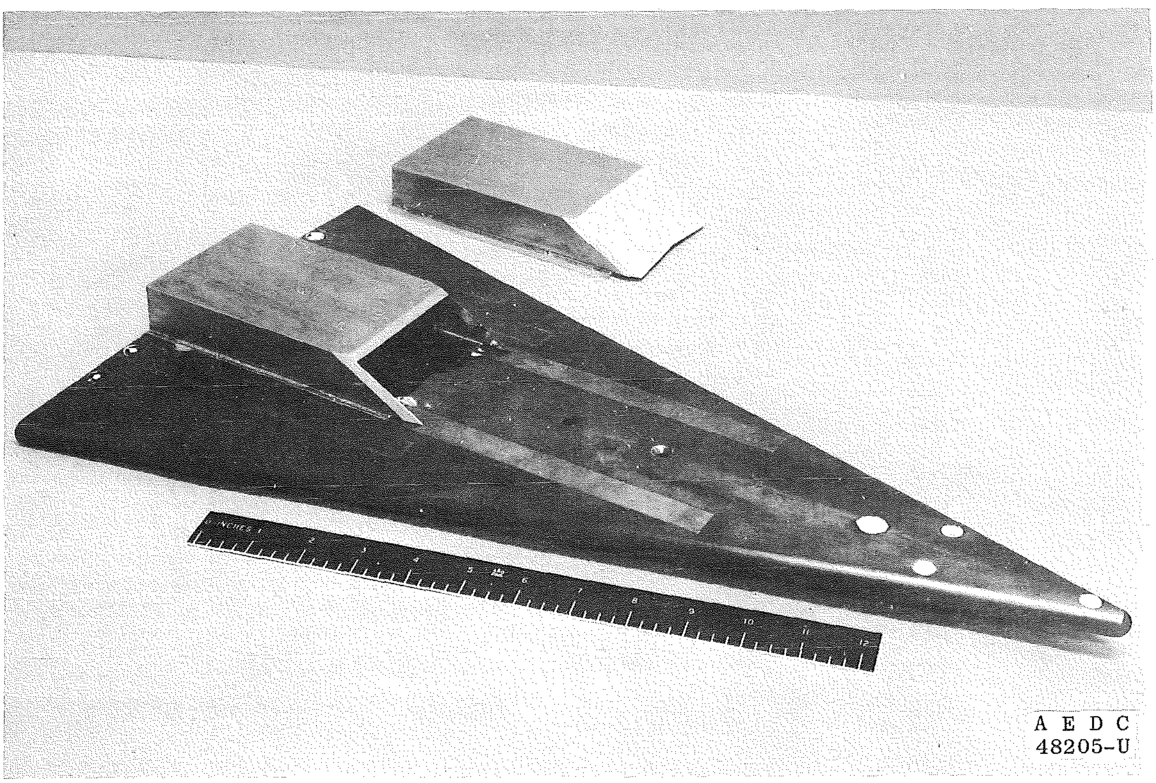

f. Configurations WB-3I$_5$ and WB-3I$_{5A}$

Fig. 2 Continued

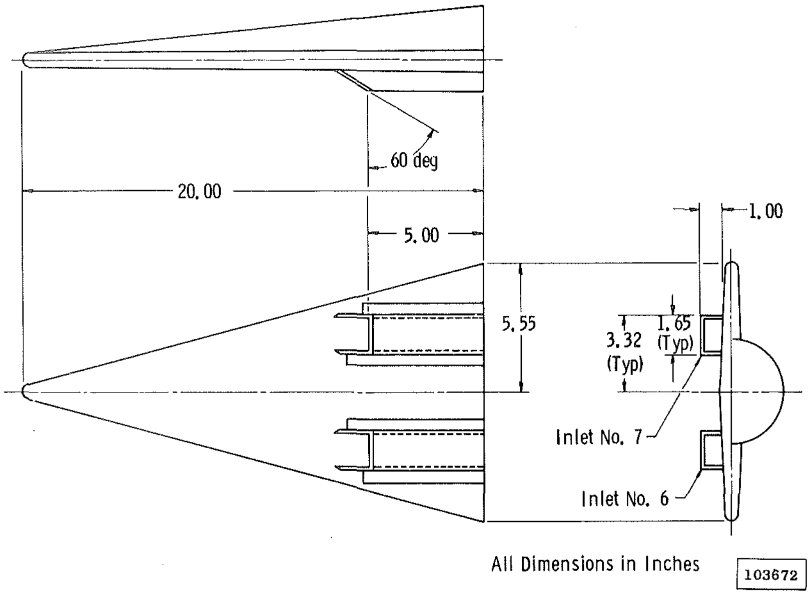

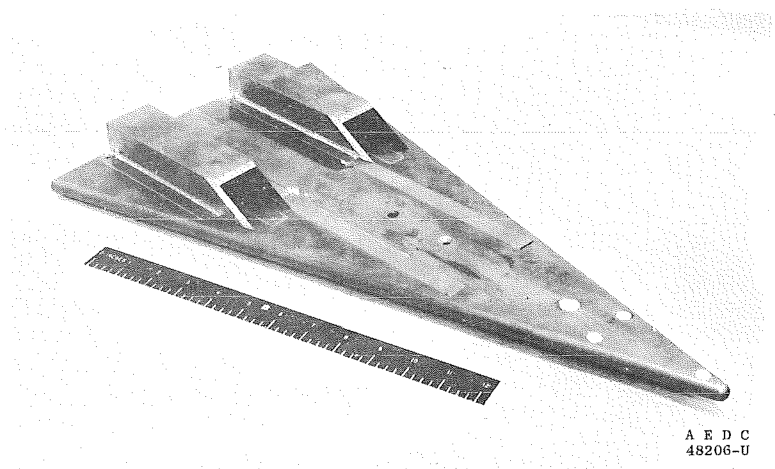

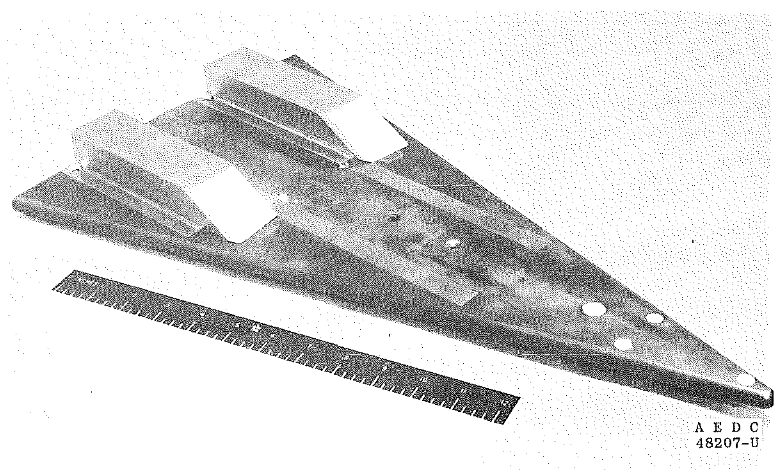

g. Configurations WB-3I_{6-7} and WB-3I_{6A-7A}

Fig. 2 Continued

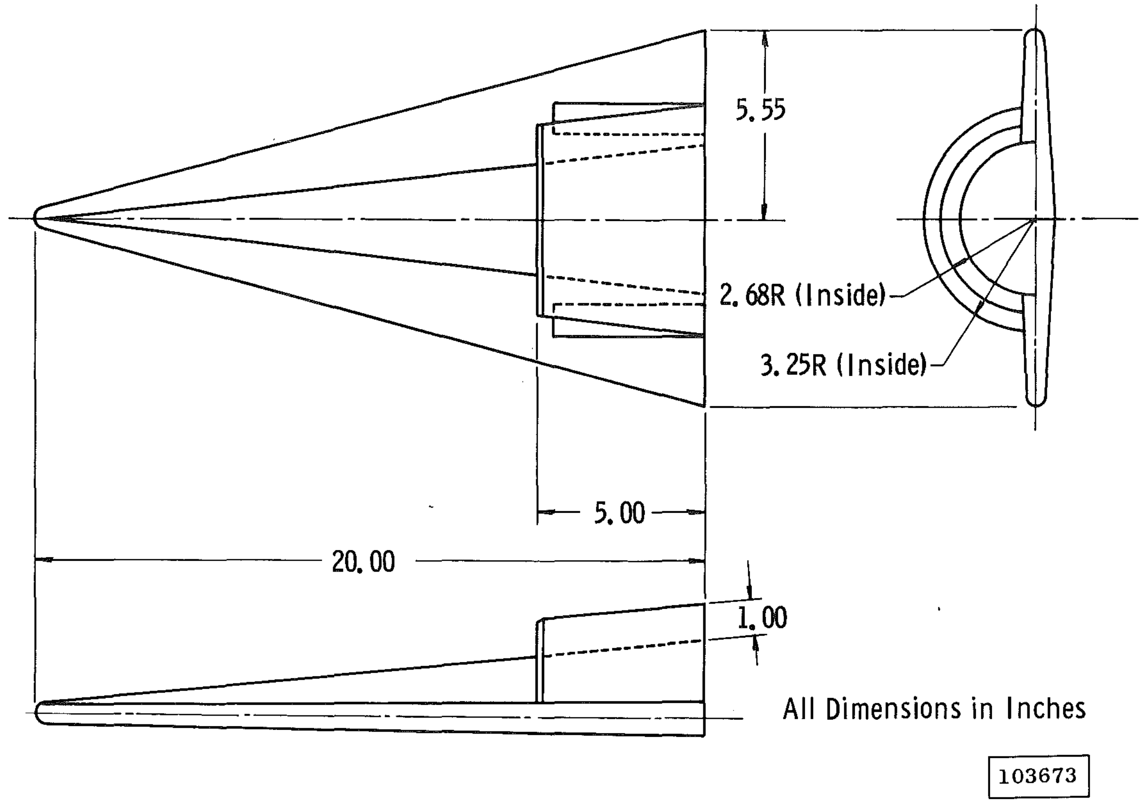

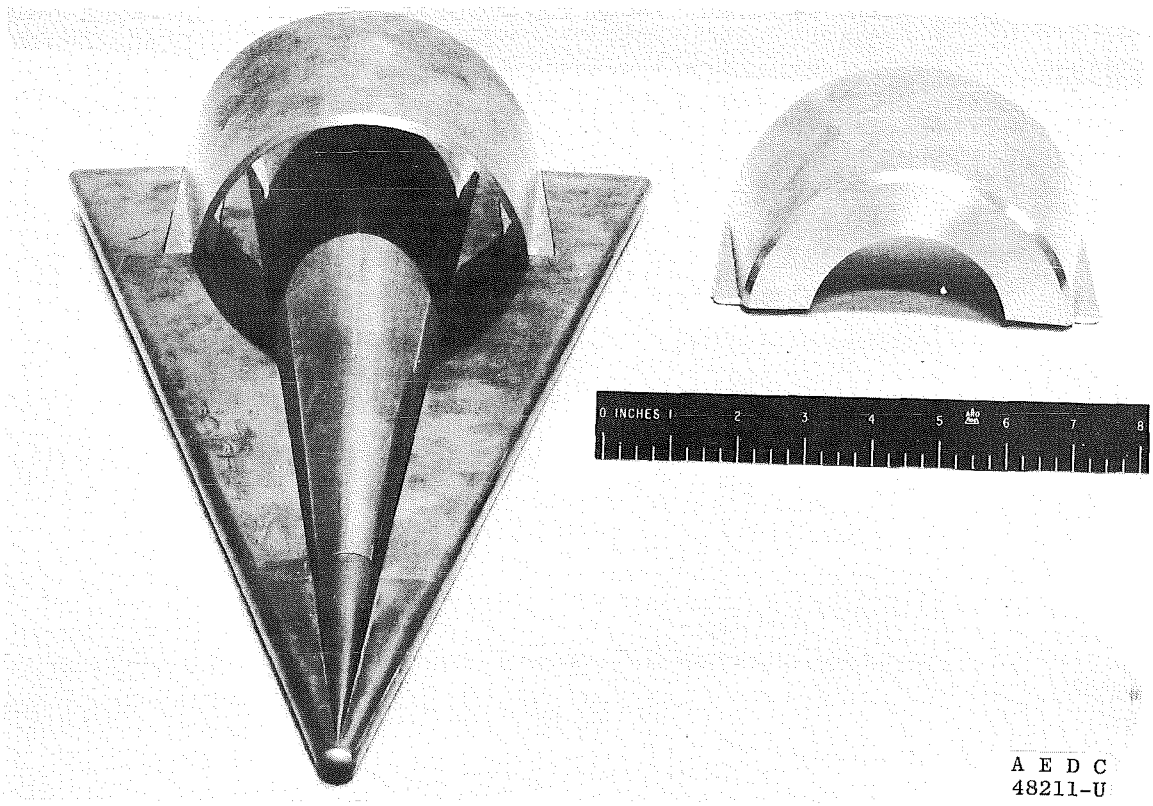

h. Configurations WB-3I$_8$ and WB-3I$_{8A}$

Fig. 2 Concluded

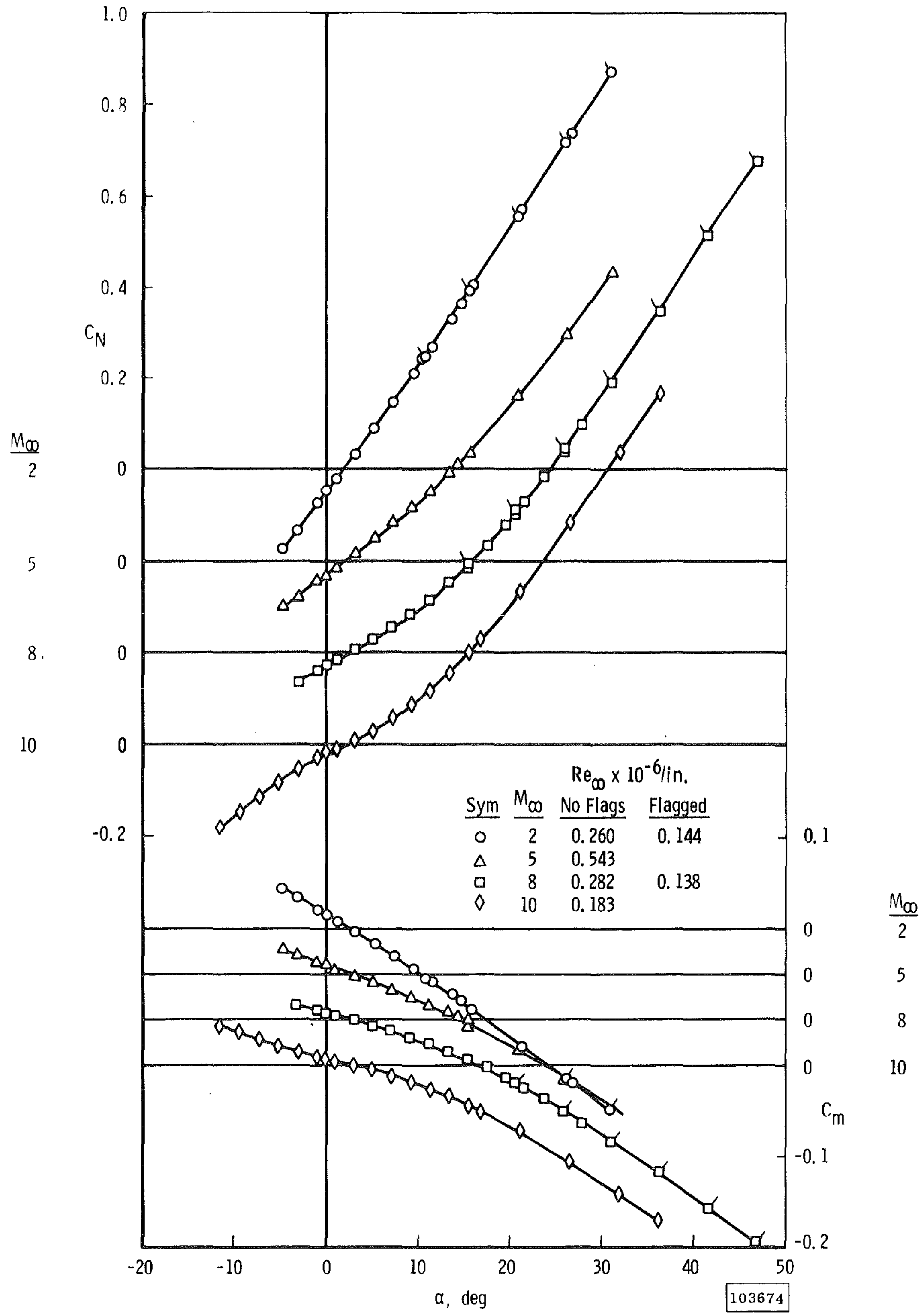

a. Variation of C_N and C_m with α

Fig. 3 Aerodynamic Characteristics of Configuration WB-3

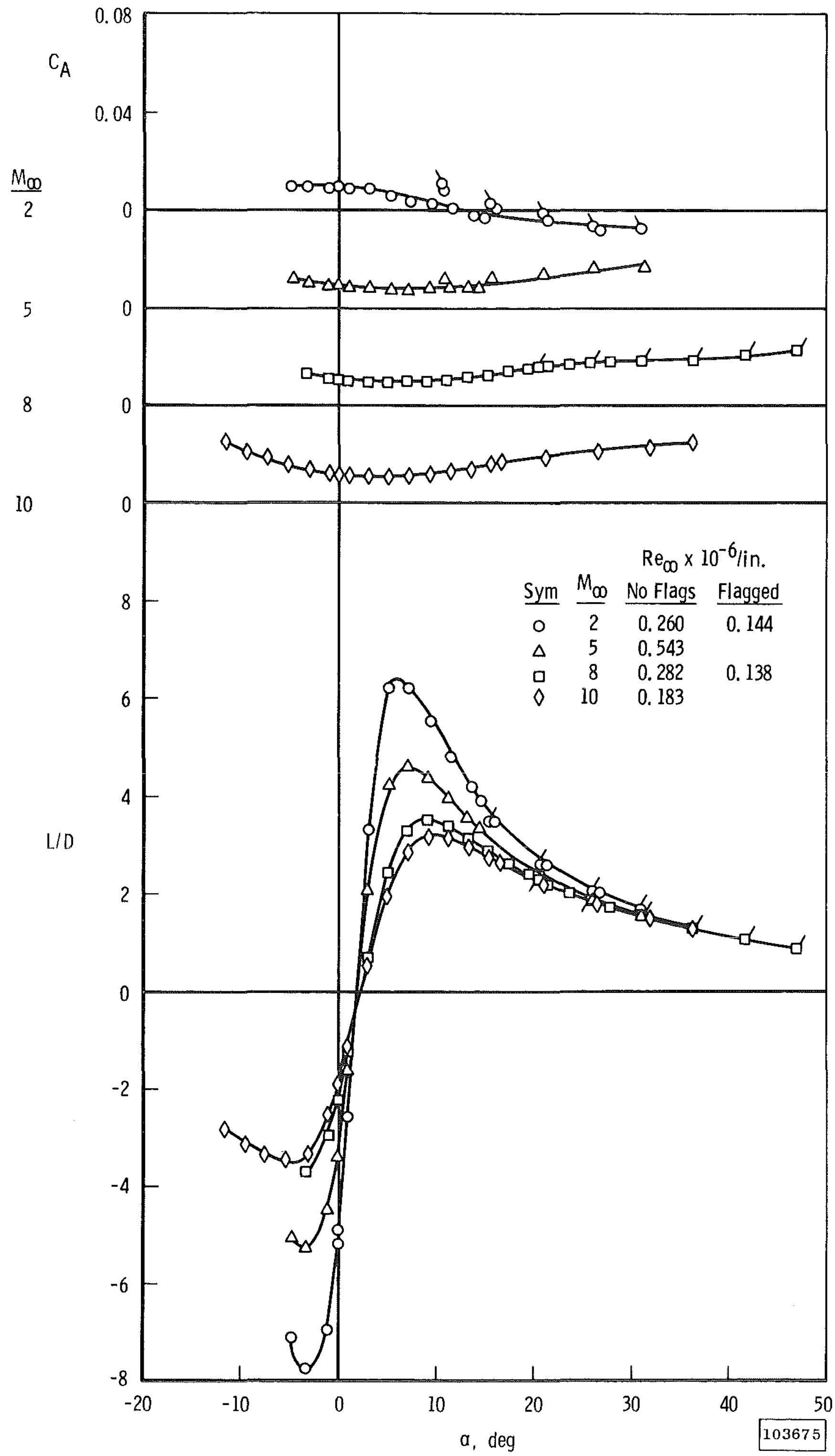

b. Variation of C_A and L/D with α

Fig. 3 Concluded

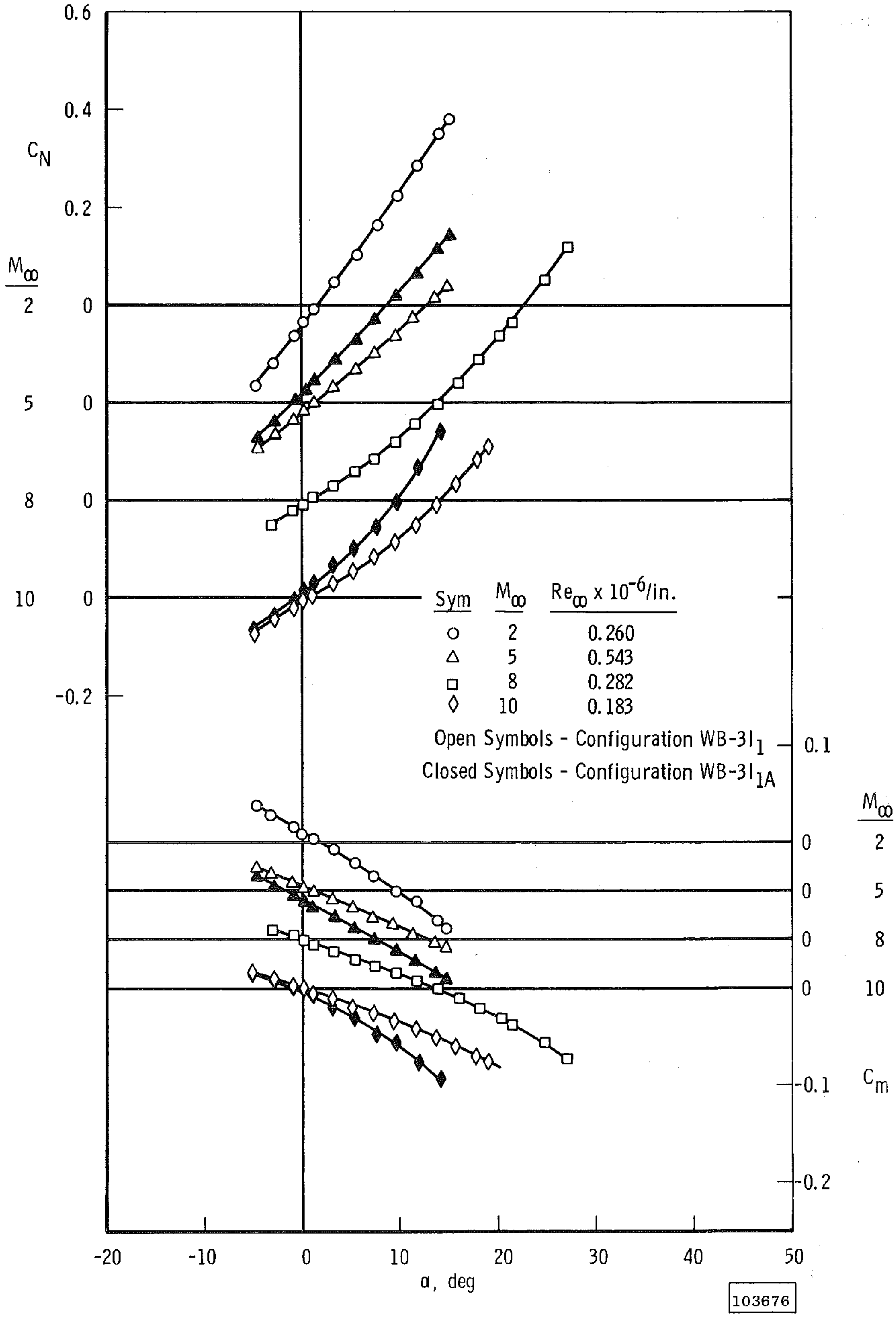

a. Variation of C_N and C_m with α

Fig. 4 Aerodynamic Characteristics of Configurations WB-3I_1 and WB-3I_{1A}

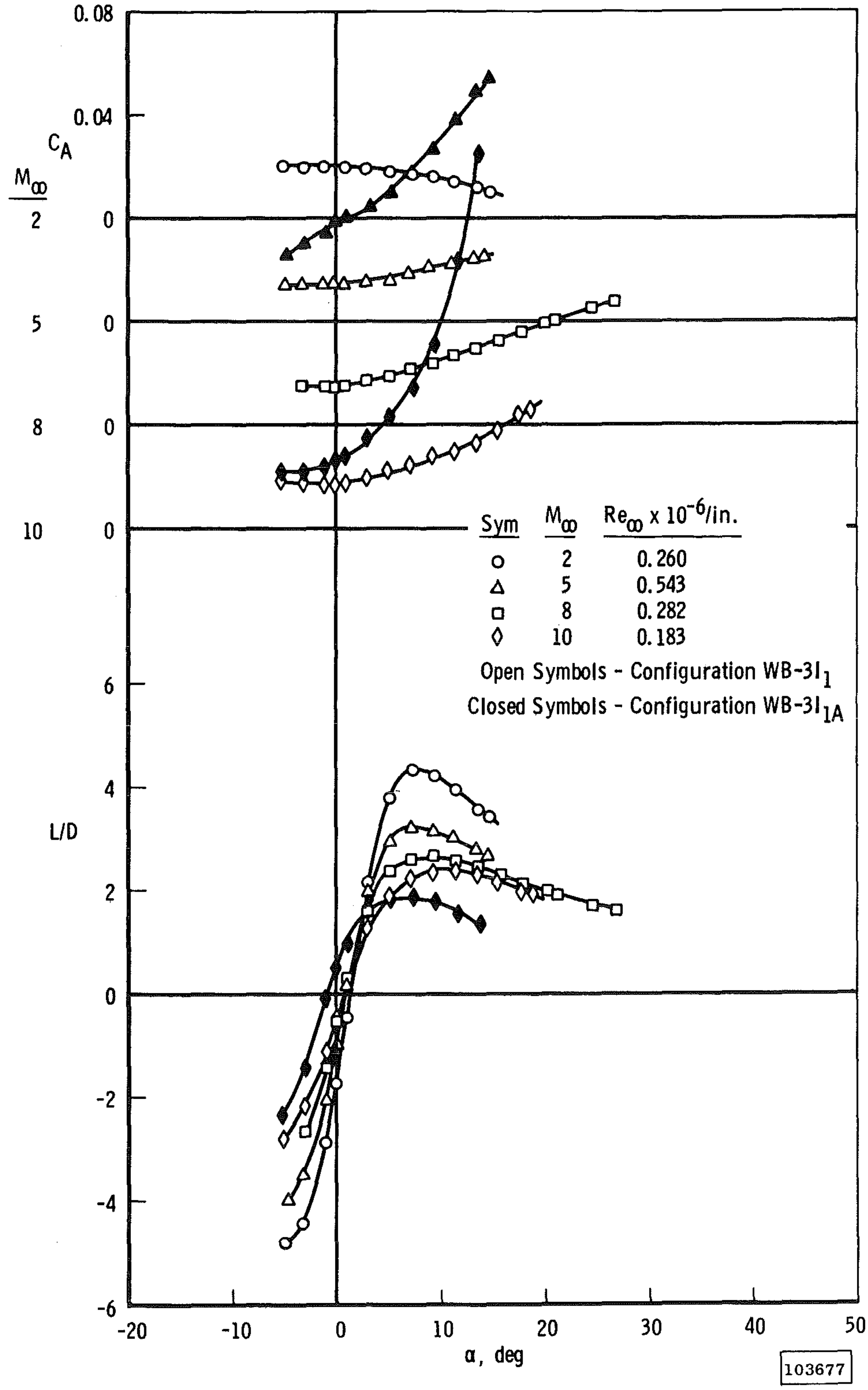

b. Variation of C_A and L/D with α

Fig. 4 Concluded

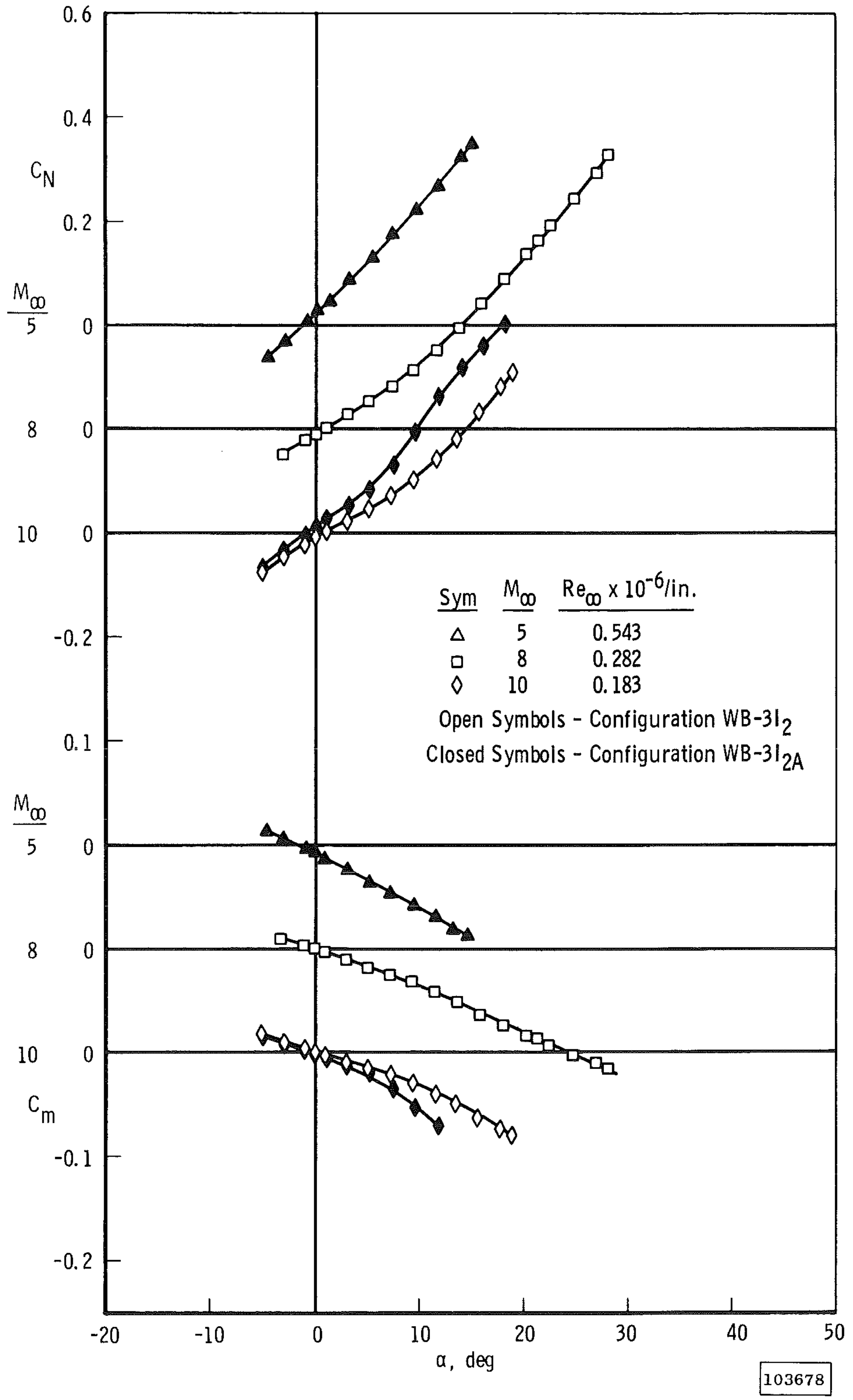

a. Variation of C_N and C_m with α

Fig. 5 Aerodynamic Characteristics of Configurations WB-3I$_2$ and WB-3I$_{2A}$

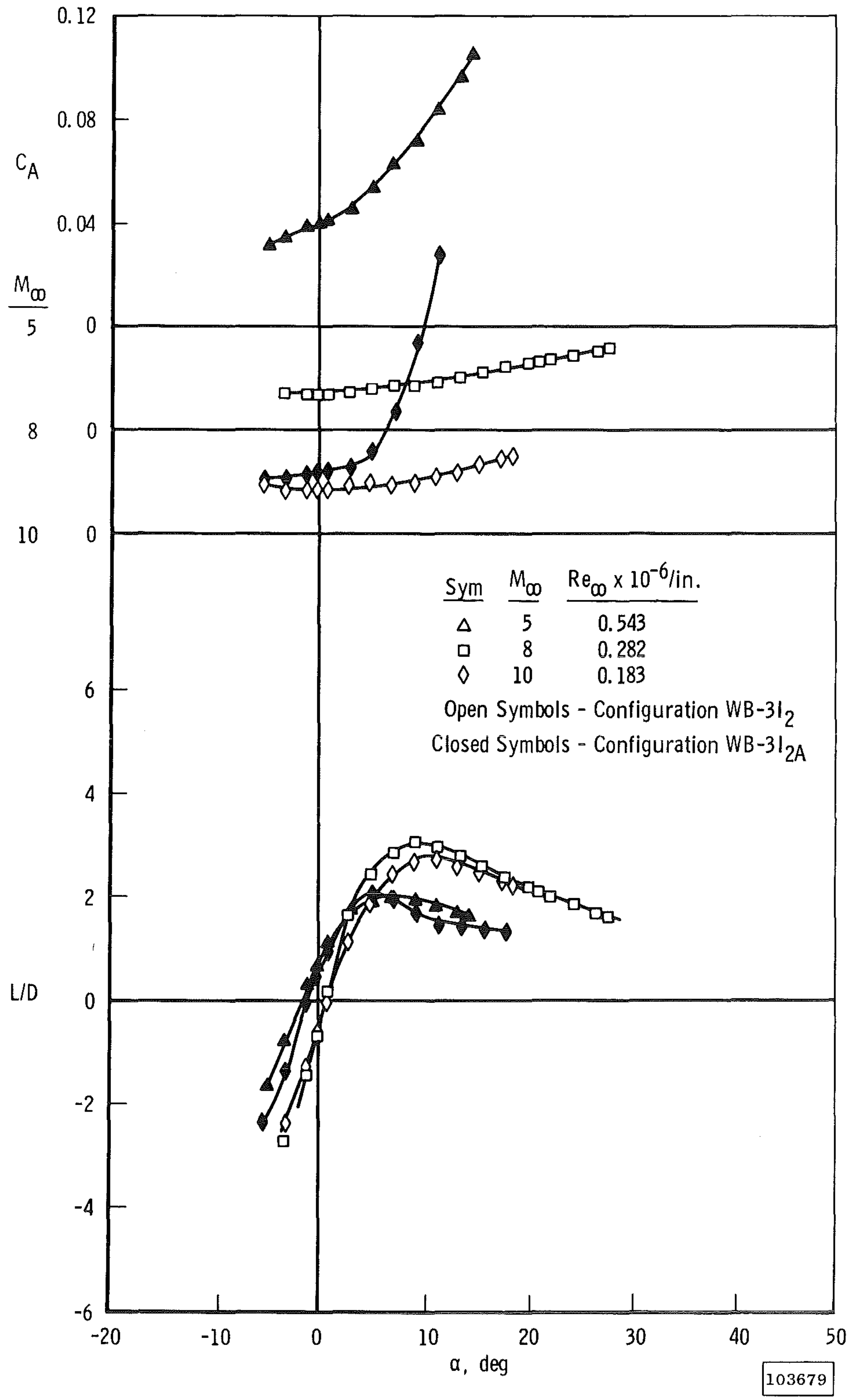

b. Variation of C_A and L/D with α

Fig. 5 Concluded

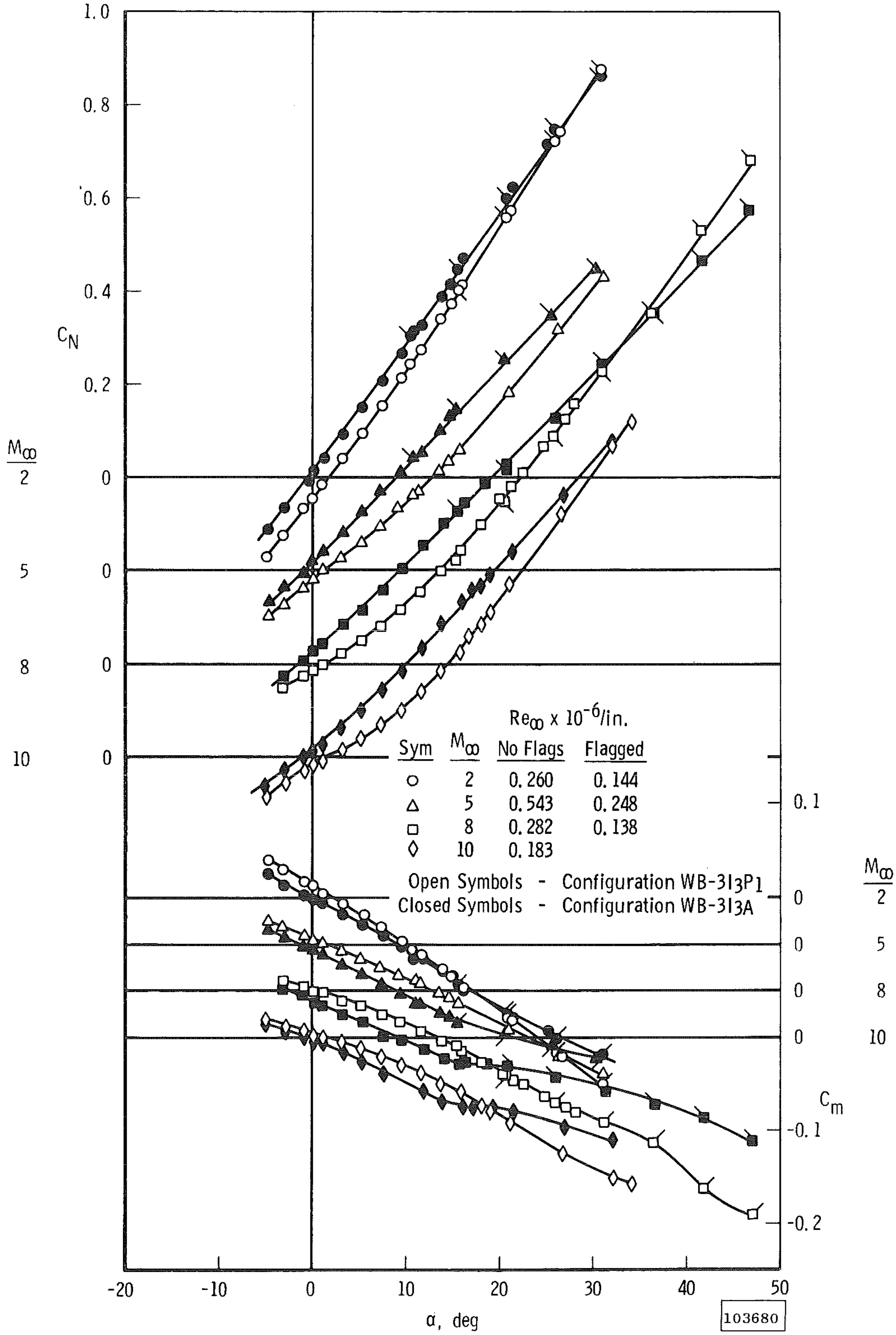

a. Variation of C_N and C_m with α

Fig. 6 Aerodynamic Characteristics of Configurations WB-3$1_3$ P_1 and WB-3$1_{3A}$

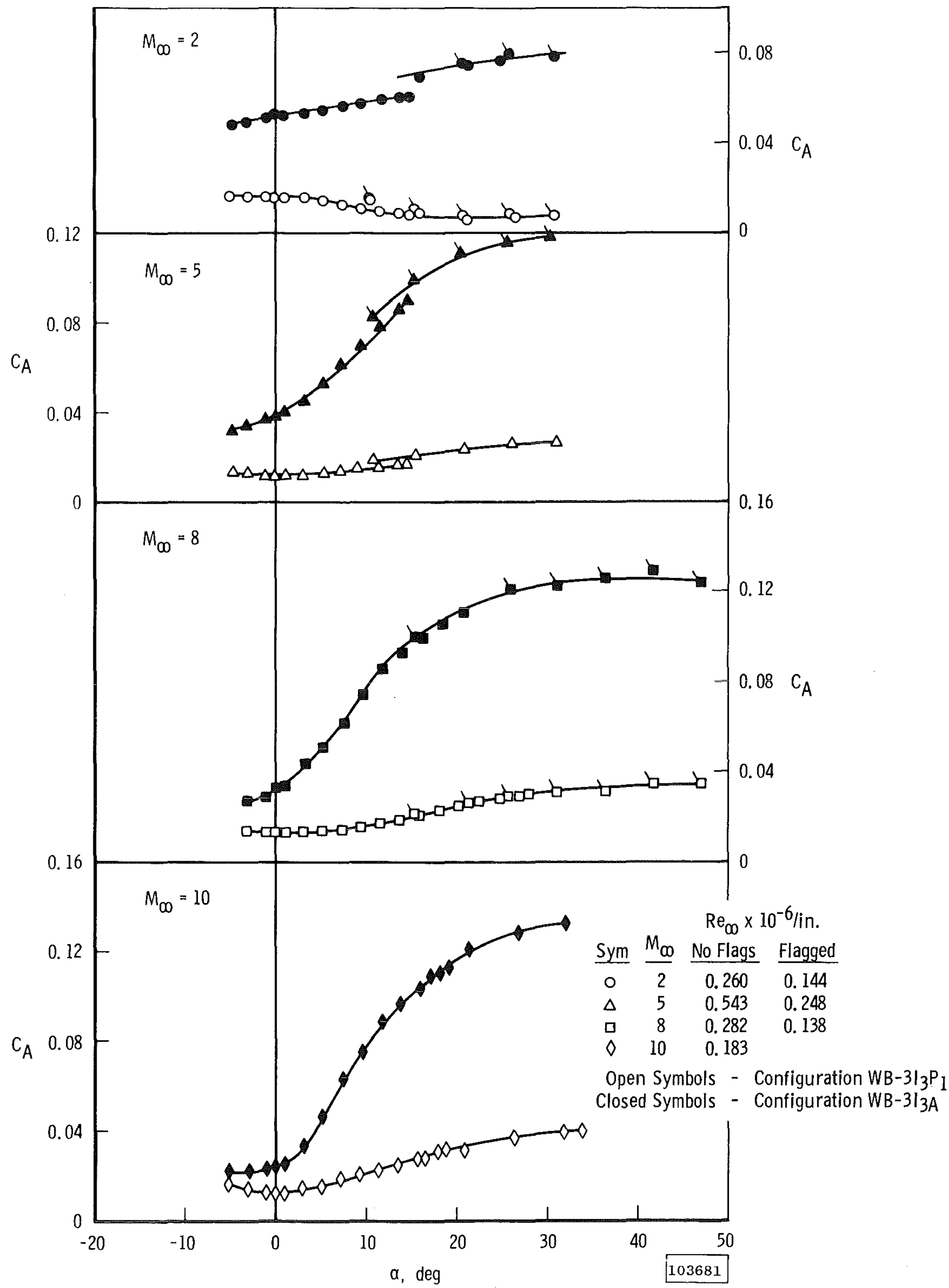

b. Variation of C_A with α

Fig. 6 Continued

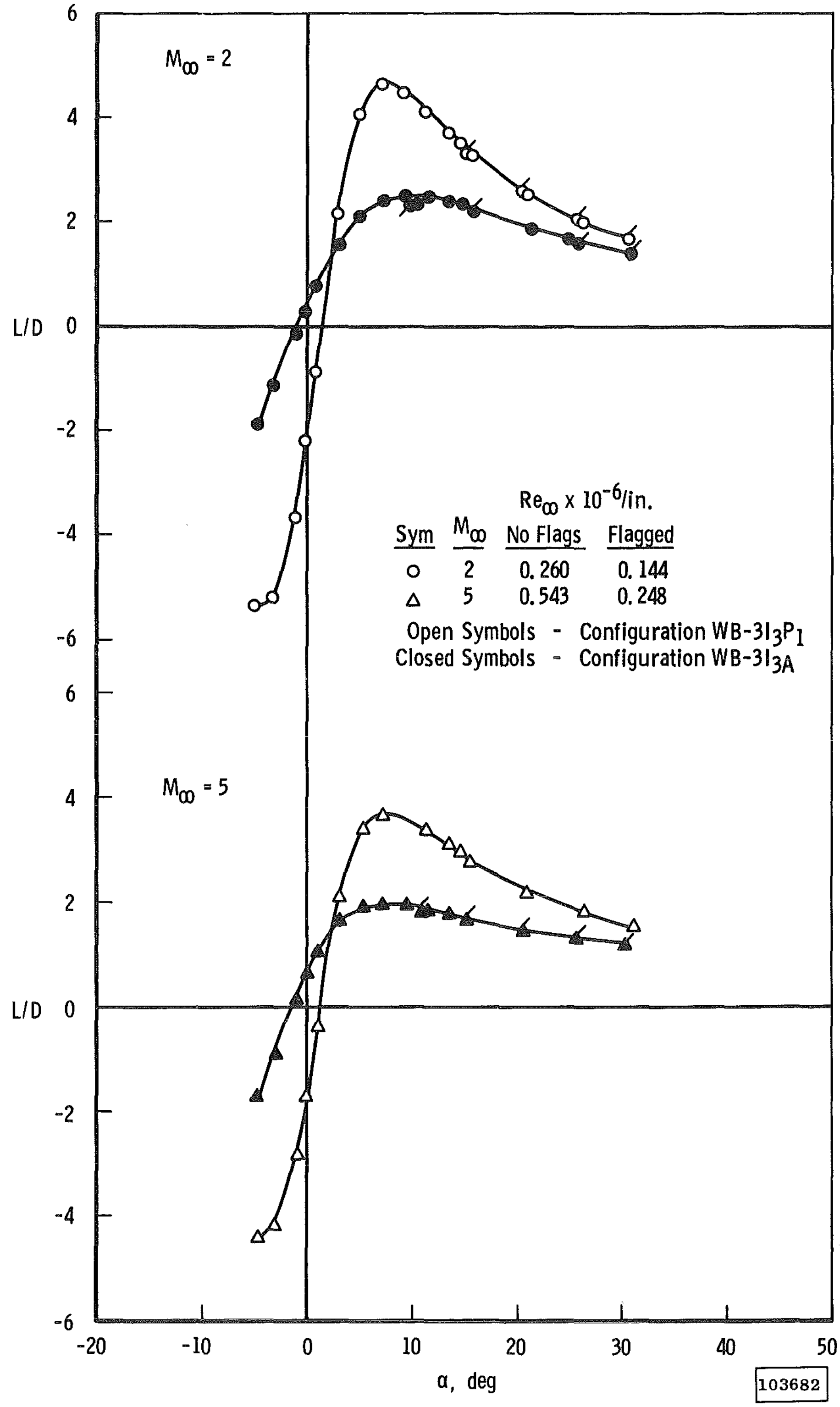

c. Variation of L/D with α (M_∞ = 2 and 5)

Fig. 6 Continued

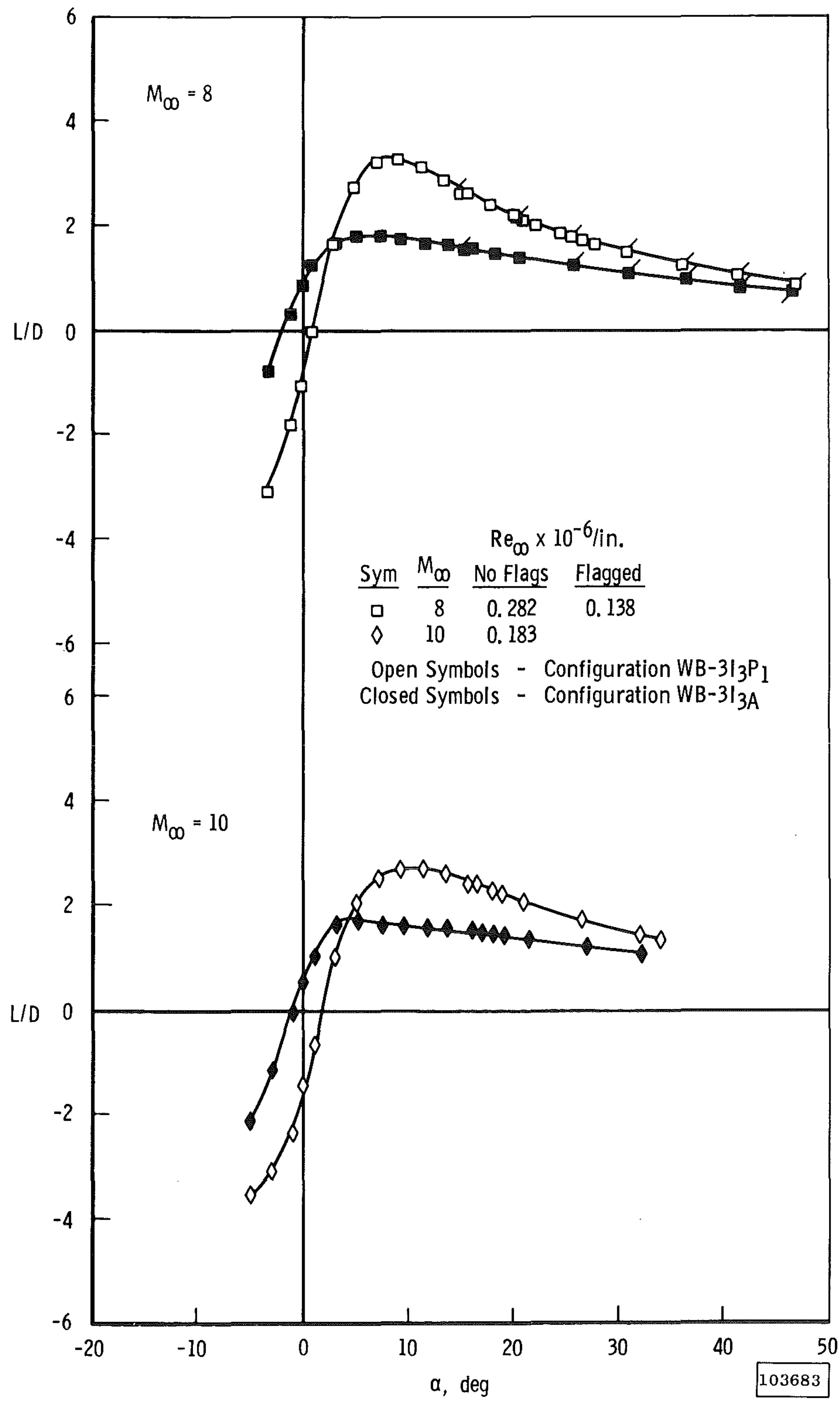

d. Variation of L/D with α (M_∞ = 8 and 10)

Fig. 6 Concluded

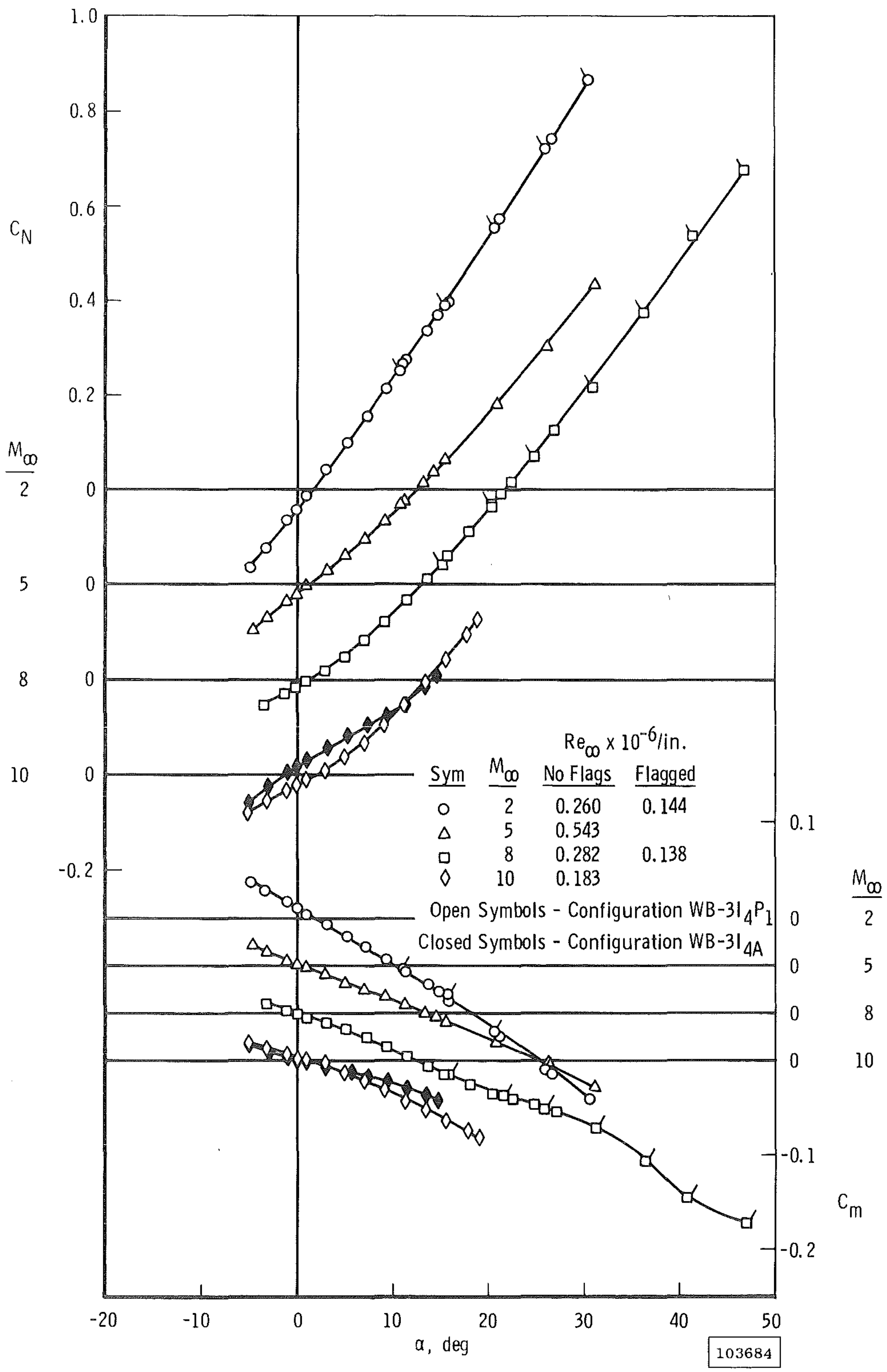

a. Variation of C_N and C_m with α

Fig. 7 Aerodynamic Characteristics of Configurations WB-3I_4P_1 and WB-3I_{4A}

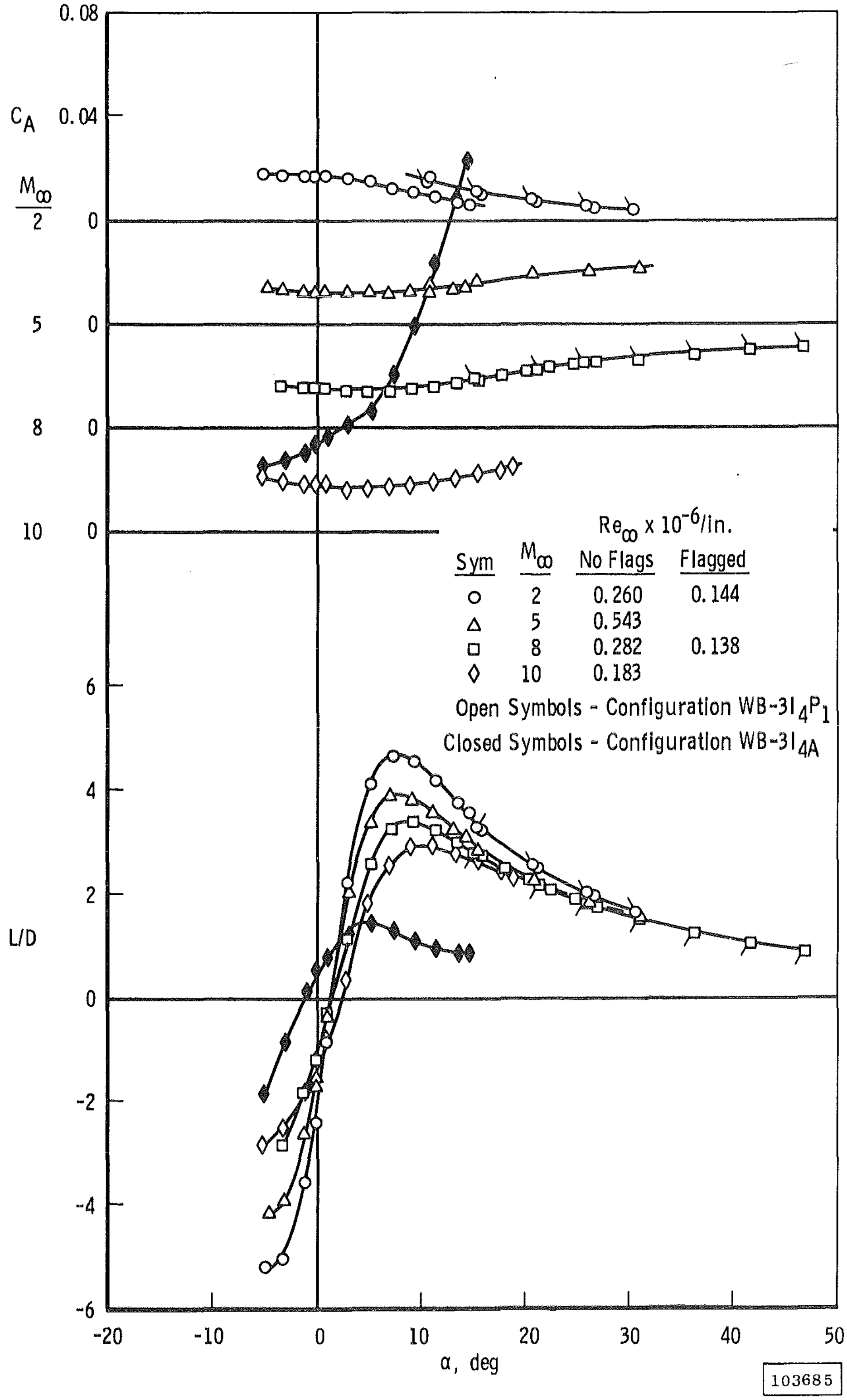

b. Variation of C_A and L/D with α

Fig. 7 Concluded

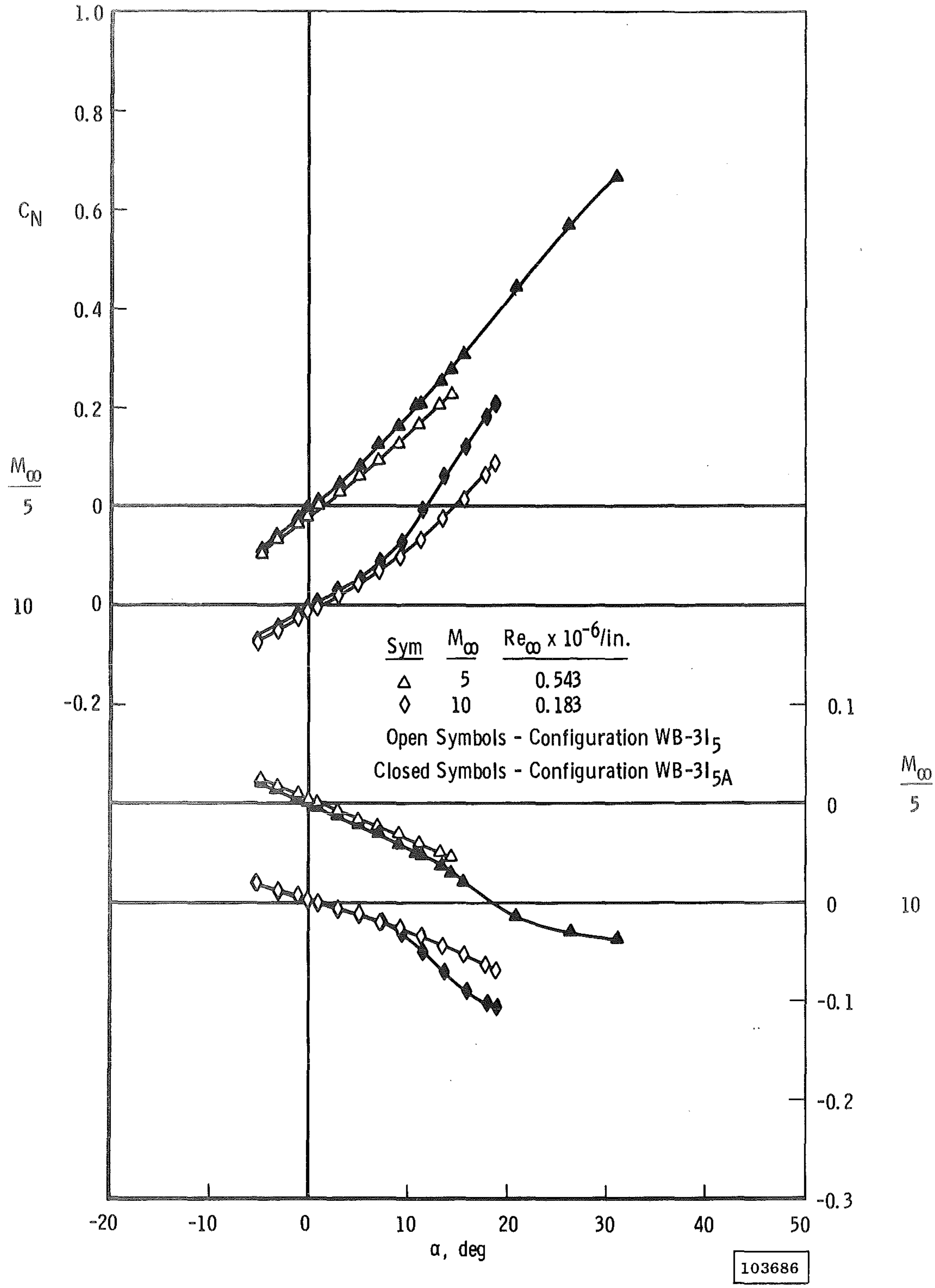

a. Variation of C_N and C_m with α

Fig. 8 Aerodynamic Characteristics of Configurations WB-3I$_5$ and WB-3I$_{5A}$

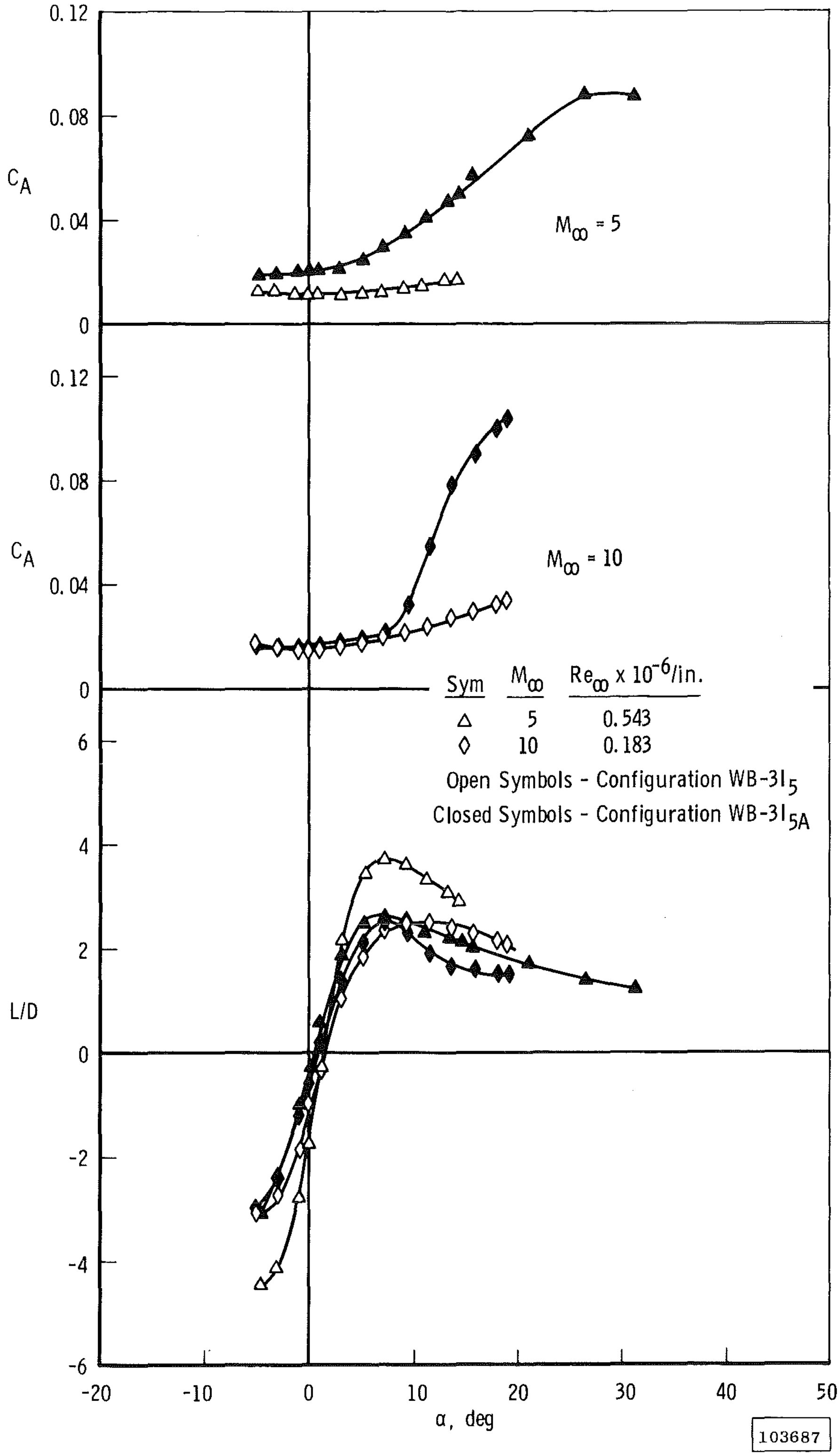

b. Variation of C_A and L/D with α

Fig. 8 Concluded

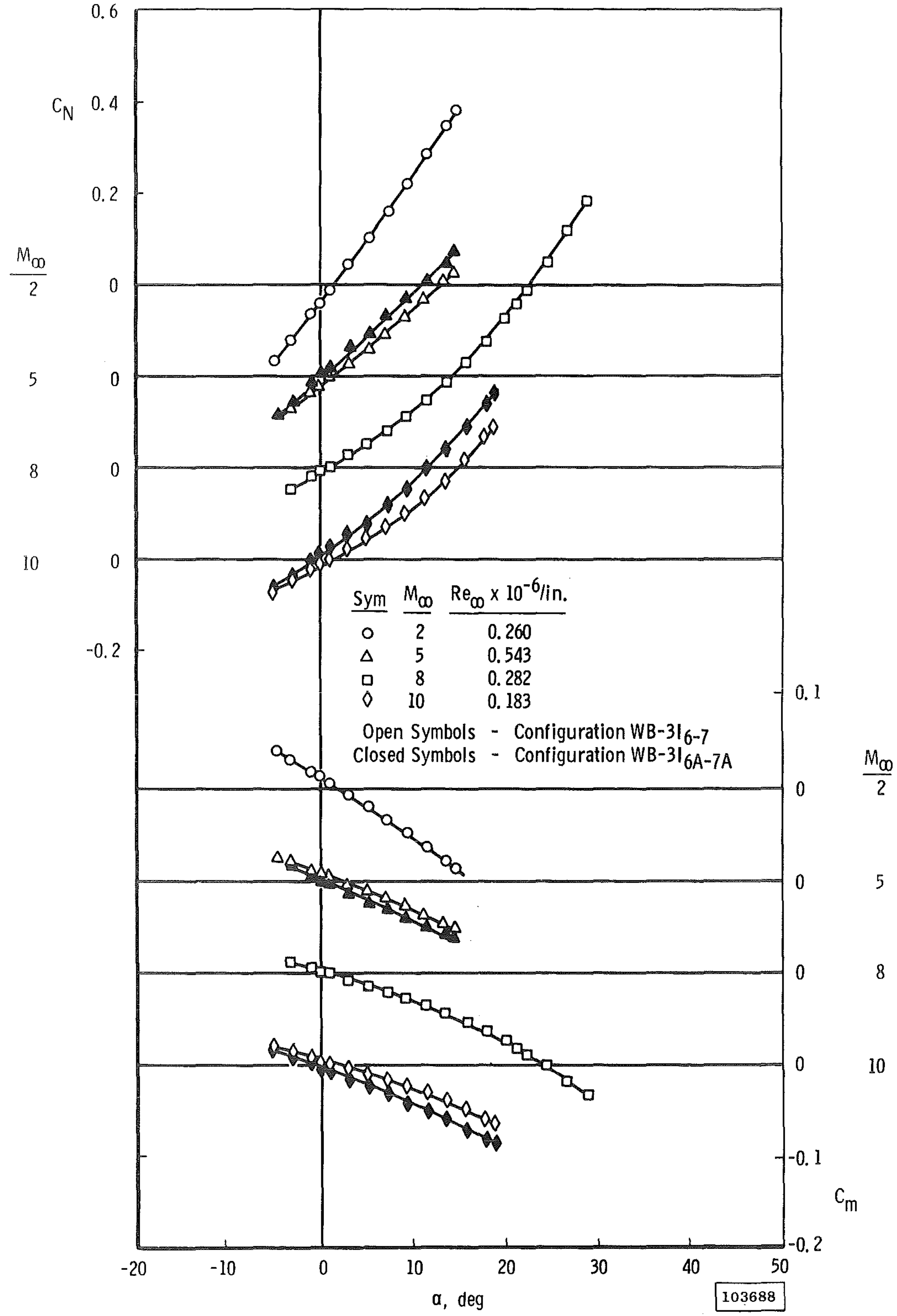

a. Variation of C_N and C_m with α

Fig. 9 Aerodynamic Characteristics of Configurations WB-3I$_{6-7}$ and WB-3I$_{6A-7A}$

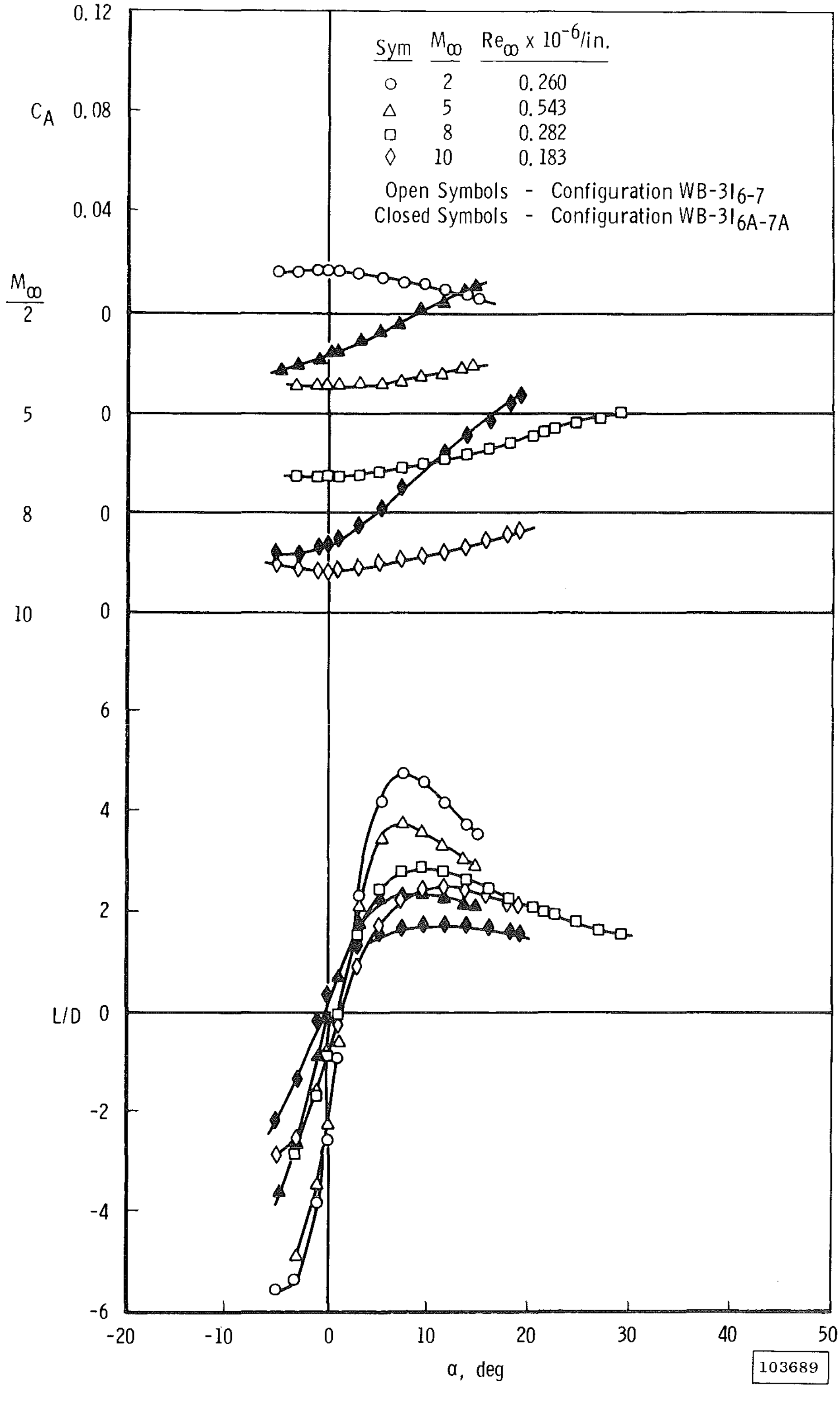

b. Variation of C_A and L/D with α

Fig. 9 Concluded

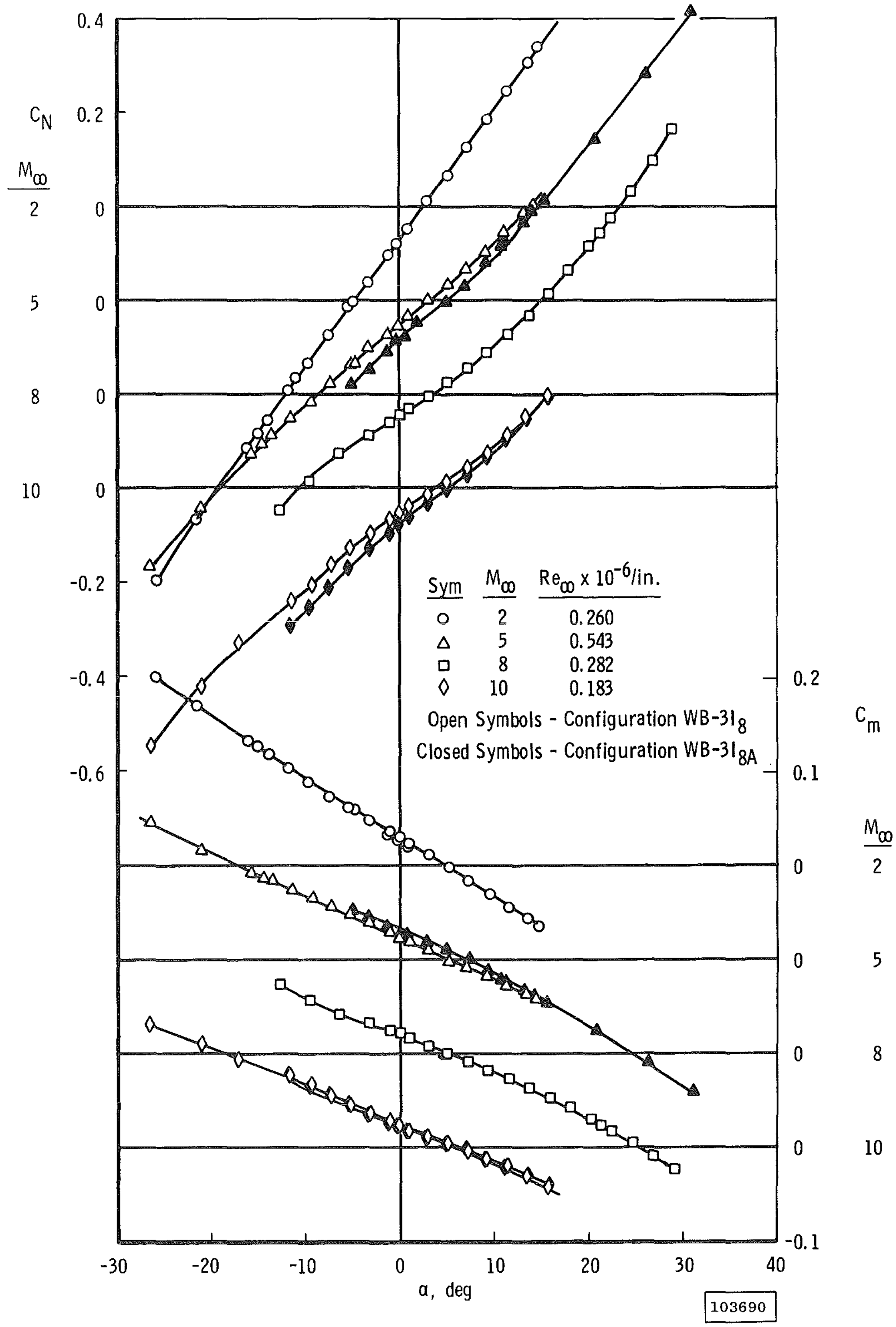

a. Variation of C_N and C_m with α

Fig. 10 Aerodynamic Characteristics of Configurations WB-3I_8 and WB-3I_{8A}

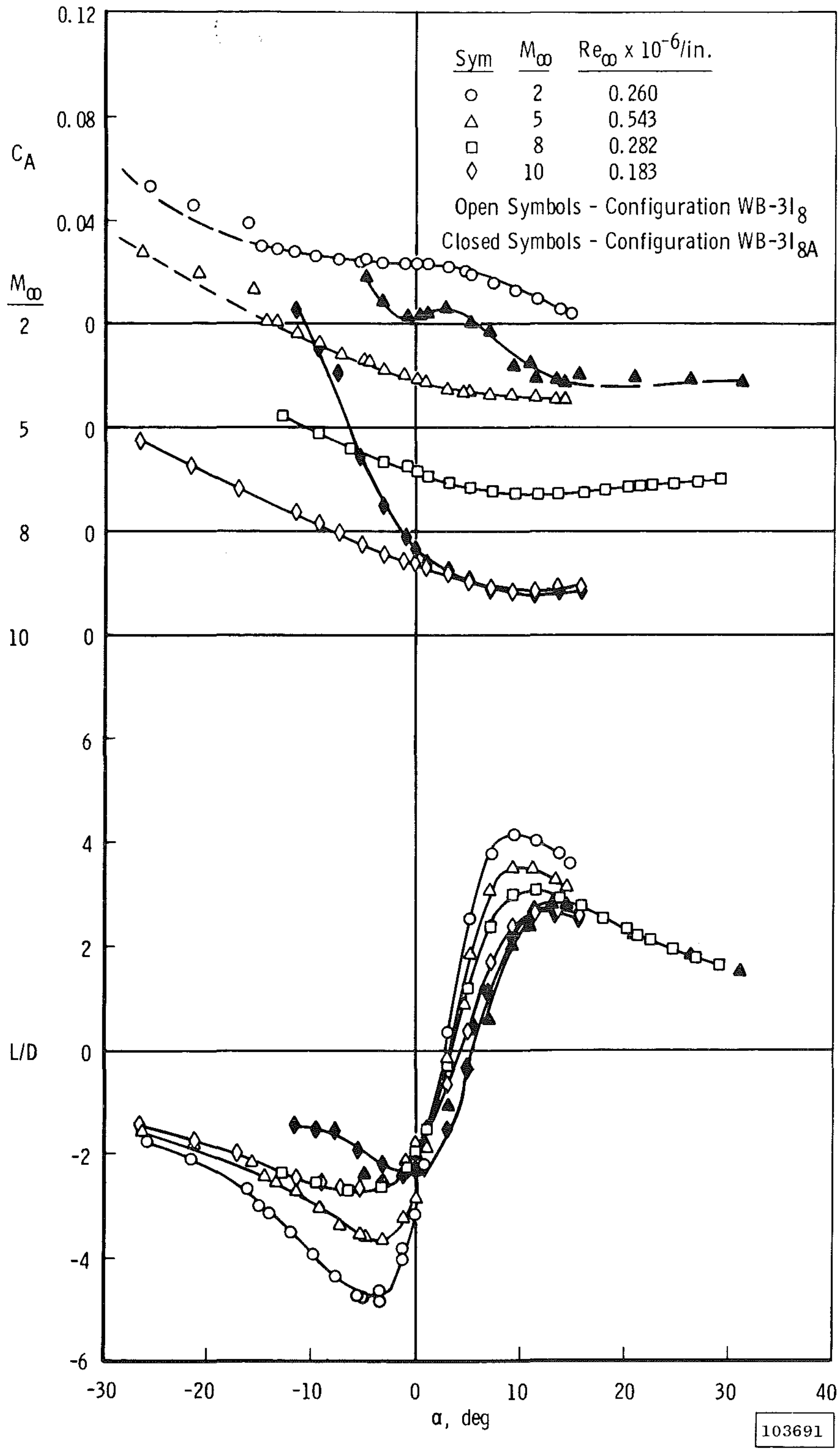

b. Variation of C_A and L/D with α

Fig. 10 Concluded

Sym	Configuration	M_∞	$Re_\infty \times 10^{-6}$/in.
○	WB-$3I_3P_1$	8	0.282
□	WB-$3I_3P_2$	10	0.183
△	WB-$3I_3P_3$		

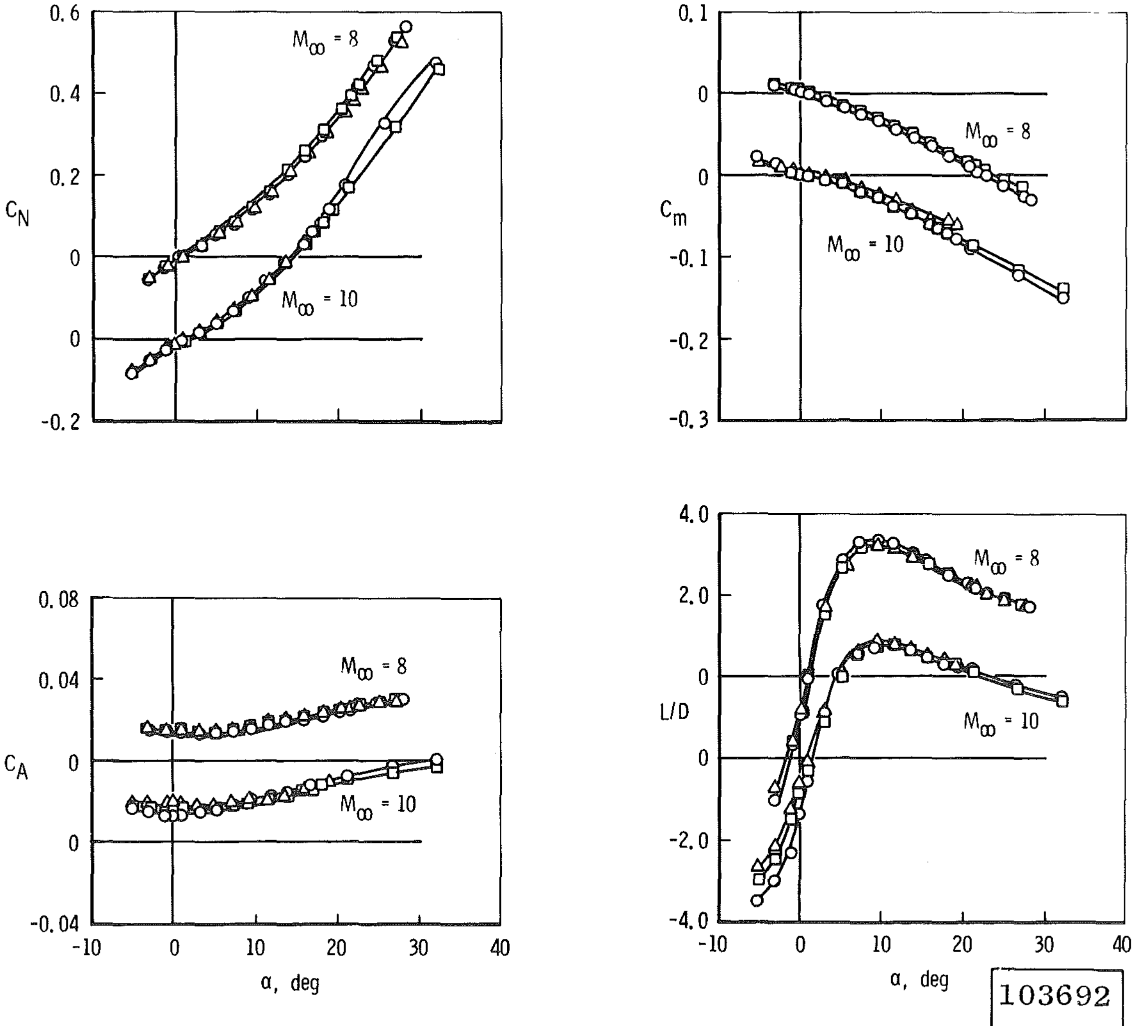

a. Inlet Number 3

Fig. 11 Effect of Inlet Position on Aerodynamic Characteristics

Sym	Configuration	M_∞	$Re_\infty \times 10^{-6}$/in.
○	$WB\text{-}3I_4P_1$	8	0.282
□	$WB\text{-}3I_4P_3$	10	0.183

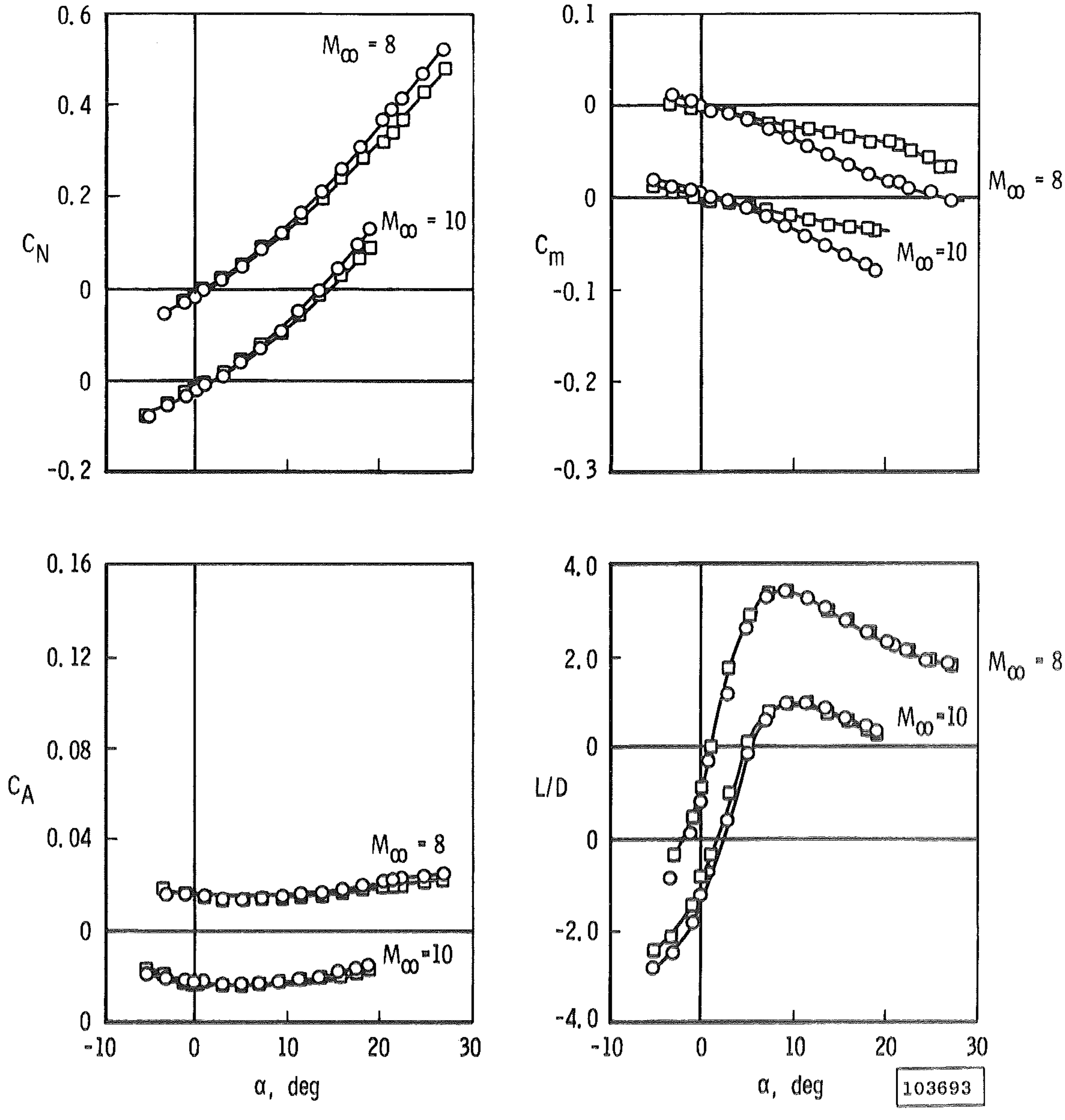

b. Inlet Number 4

Fig. 11 Concluded

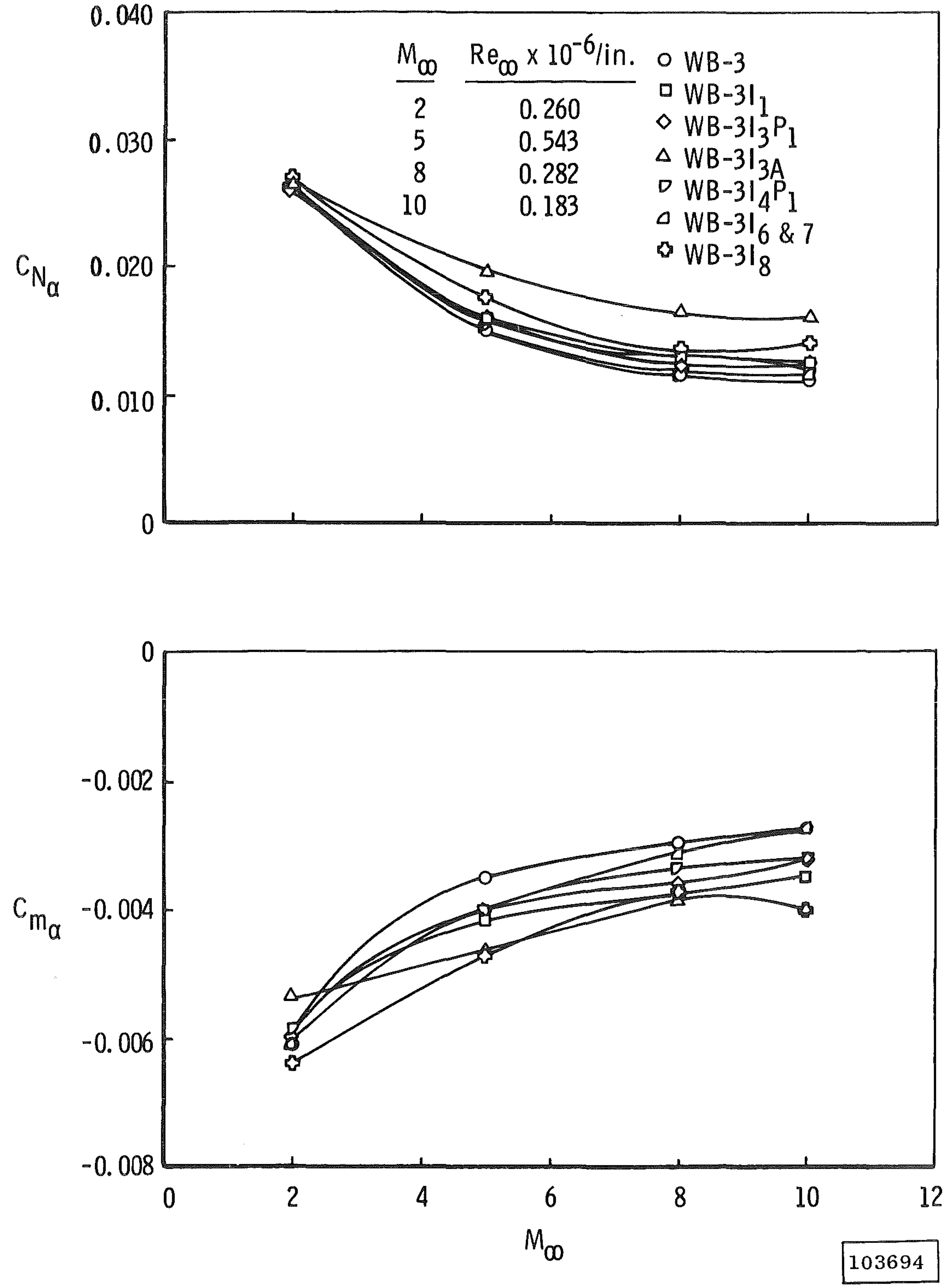

a. Variation of C_{N_α} and C_{m_α} with M_∞

Fig. 12 Effect of Mach Number on Stability and Drag Characteristics

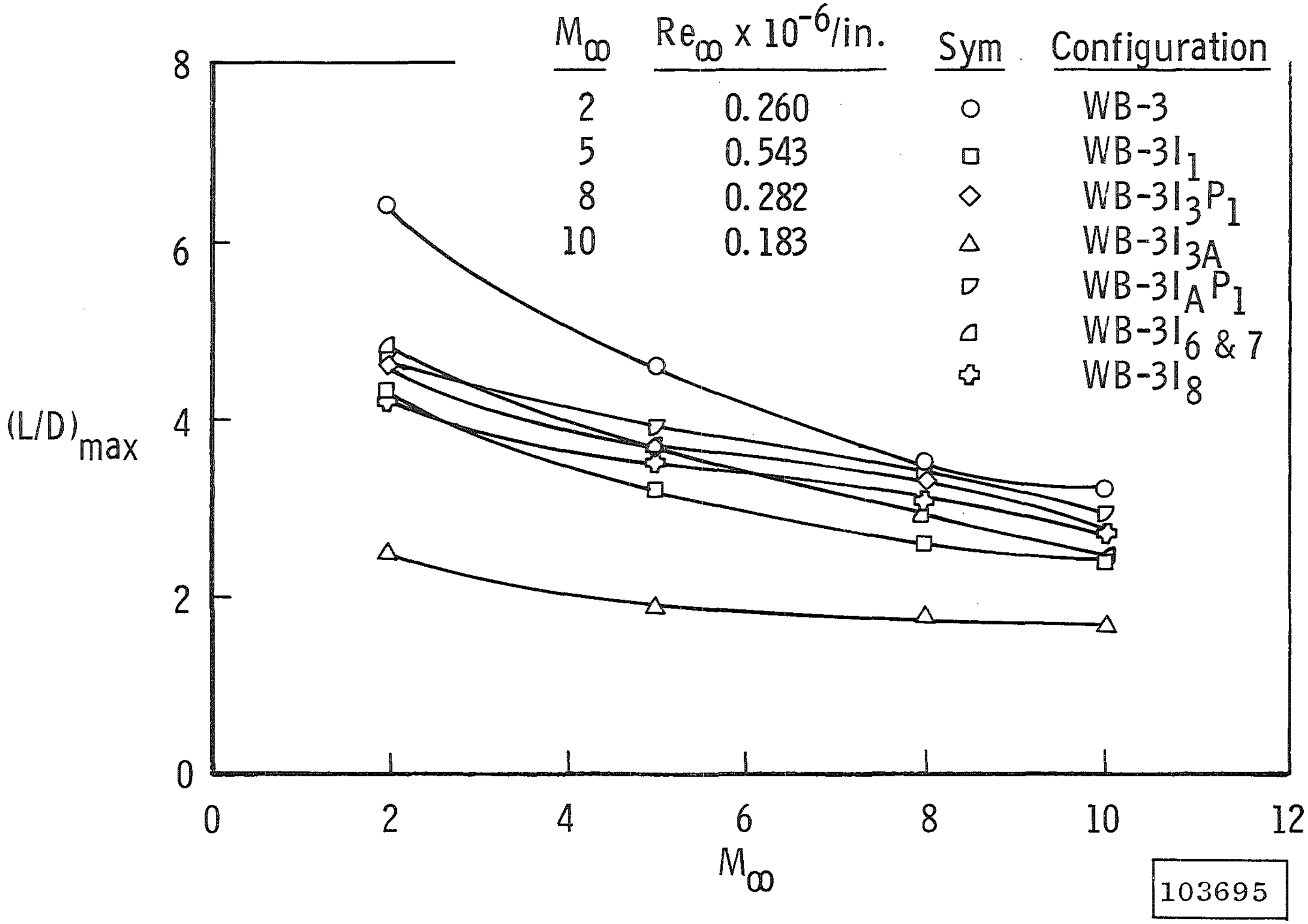

b. Variation of $(L/D)_{max}$ with M_∞

Fig. 12 Concluded

~~CONFIDENTIAL~~
DECLASSIFIED / UNCLASSIFIED